JCI The Journal of Clinical Investigation

Thrombocytopenia-associated mutations in Ser/Thr kinase MASTL deregulate actin cytoskeleton dynamics in platelets

Begoña Hurtado, … , Pablo García de Frutos, Marcos Malumbres

J Clin Invest. 2018. https://doi.org/10.1172/JCI121876.

Research | In-Press Preview | Cell biology | Hematology

Graphical abstract

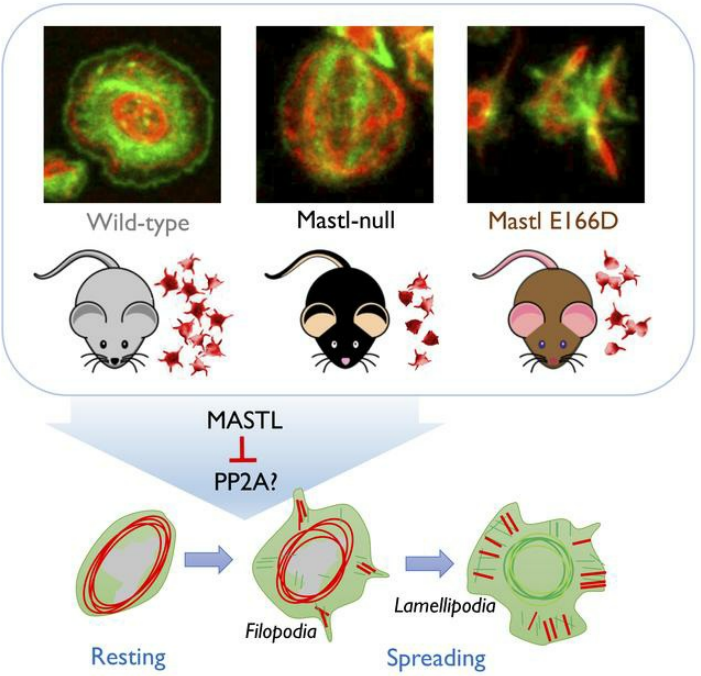

Thrombocytopenia-associated mutations in Ser/Thr kinase MASTL deregulate actin cytoskeleton dynamics in platelets

Begoña Hurtado,[1,2*] Marianna Trakala,[1*] Pilar Ximénez-Embún,[3] Aicha El Bakkali,[1] David Partida,[1] Belén Sanz-Castillo,[1] Mónica Álvarez-Fernández,[1] María Maroto,[1] Ruth Sánchez-Martínez,[1] Lola Martínez[4], Javier Muñoz,[3] Pablo García de Frutos[2] and Marcos Malumbres[1,‡]

* These authors contributed equally to this work.

[1] *Cell Division and Cancer Group, Spanish National Cancer Research Centre (CNIO) Madrid, Spain*

[2] *Department of Cell Death and Proliferation, IIBB-CSIC, IDIBAPS, Barcelona, Spain*

[3] *ProteoRed-ISCIII and Proteomics Unit, CNIO, Madrid, Spain*

[4] *Cytometry Unit, CNIO, Madrid, Spain*

[‡] *Correspondence*: M. Malumbres. Centro Nacional de Investigaciones Oncológicas (CNIO), Melchor Fernández Almagro 3, E-28029 Madrid, Spain. Tel. +34 91 732 8000, Fax +34 91 732 8033; E-mail: malumbres@cnio.es

The authors have declared that no conflict of interest exists.

ABSTRACT

MASTL, a Ser/Thr kinase that inhibits PP2A-B55 complexes during mitosis, is mutated in autosomal dominant thrombocytopenia. However, the connections between the cell cycle machinery and this human disease remain unexplored. We report here that, whereas *Mastl* ablation in megakaryocytes prevented proper maturation of these cells, mice carrying the thrombocytopenia-associated mutation developed thrombocytopenia as a consequence of aberrant activation and survival of platelets. Activation of mutant platelets was characterized by hyper-stabilized pseudopods mimicking the effect of PP2A inhibition and actin polymerization defects. These aberrations were accompanied by abnormal hyper-phosphorylation of multiple components of the actin cytoskeleton and were rescued both in vitro and in vivo by inhibiting upstream kinases such as PKA, PKC or AMPK. These data reveal an unexpected role of Mastl in actin cytoskeleton dynamics in postmitotic cells, and suggest that the thrombocytopenia-associated mutation in MASTL is a pathogenic dominant mutation that mimics decreased PP2A activity resulting in altered phosphorylation of cytoskeletal regulatory pathways.

INTRODUCTION

Mastl (Microtubule-Associated Serine/Threonine protein kinase-Like; also known as Greatwall) is a recently characterized kinase with critical functions in the maintenance of mitosis (1, 2). This kinase was originally discovered in *Drosophila* screenings for cell cycle mutants (3-5), and was later shown to phosphorylate endosulfine (Ensa) and Arpp19, two small proteins that when phosphorylated function as PP2A-B55 inhibitors (6, 7). Depletion of Greatwall in flies and *Xenopus* leads to defective chromosome condensation and segregation, as a consequence of the hyperactivation of PP2A-B55 complexes, and the subsequent dephosphorylation of cyclin-dependent kinase 1 (Cdk1) substrates (4, 8). Less is known about the physiological relevance of the mammalian Mastl orthologue although knockdown and knockout assays suggest that it also participates in chromosome condensation and the maintenance of the mitotic state in a PP2A-B55-dependent manner (9-13).

Before the functional role of Mastl was studied in mammalian cells, a missense mutation in the human *MASTL* locus (located in chromosome 10p11-12) was found to perfectly segregate with nonsyndromic autosomal dominant thrombocytopenia, also known as thrombocytopenia-2 (THC2) (14). These patients were characterized by incomplete differentiation of megakaryocytes and moderate thrombocytopenia with certain propensity towards easy bruising and minor bleeding (15, 16). The mutation, a substitution of cytosine for guanidine (G to C) at nucleotide position 565, was present in all thrombocytopenic family members, causing a predicted substitution of aspartic acid for glutamic acid (E167D) in the human *MASTL* gene (14). In addition to the E167D substitution in *MASTL*, additional mutations in two genes in the THC2 region of chromosome 10p11-12 have been linked to congenital thrombocytopenia. These include

specific mutations in *ACBD5* and the 5' UTR of *ANKRD26*, the ankyrin repeat domain 26 gene (17). *ANKRD26* mutations are the most frequent finding in THC2 patients (18) and the three affected genes are very close in human chromosome 10p12.1 (*ACBD5-MASTL-YME1L1-ANKRD26*; centromeric to telomeric), raising questions on the relative contribution of *MASTL* mutations to thrombocytopenia (17, 19).

In order to get new insights into the biological significance of Mastl in mammalian tissues, we have generated mutant mice with specific ablation of the *Mastl* gene in mature megakaryocytes as well as a new knockin model carrying the thrombocytopenia-associated mutation (E166D in the mouse). This mutation in Mastl does not result in reduced activity as originally thought (14), but is accompanied by increased phosphorylation of Cdk/PP2A substrates, suggesting a gain-of-function alteration that results in decreased PP2A activity. Whereas genetic ablation of Mastl results in deficient maturation of megakaryocytes in vivo, *Mastl* E166D mutant mice display defective dynamics in the actin cytoskeleton during platelet activation accompanied by an altered pattern of protein phosphorylation. These defects can be mimicked by PP2A inhibition and partially rescued by downregulating critical kinases involving in outside-in signaling. These results suggest a specific contribution of Mastl mutations in human thrombocytopenia and unveil an unexpected function for Mastl in sustaining actin cytoskeleton in non-dividing cells, a function that may have significant implications in human disease.

RESULTS

Mastl deficiency, but not the E166D mutation, results in defective maturation in megakaryocytes

We first made use of a conditional allele [*Mastl*(lox)] generated in our laboratory (12) in which exon 4, carrying essential domains for kinase activity, can be deleted upon activation of Cre recombinase resulting in a *Mastl* null allele (Figure 1A). Since homozygous germline ablation of Mastl [*Mastl*(–/–)] results in early embryonic lethality (12), we decided to specifically ablate Mastl in mature megakaryocytes and platelets by using Pf4-Cre transgenic animals (20), thus generating Pf4-Cre; *Mastl*(Δ/Δ) mice [from now on *Mastl*(Δ/Δ)]. To mimic the alteration found in thrombocytopenia, we also generated a knockin allele carrying the orthologue mutation found in human patients (corresponding to E166D in the mouse; *Mastl*(ED) allele; Figure 1B). Whereas deletion of exon 4 in knockout *Mastl*(Δ/Δ) mice results in a frameshift preventing the generation of transcripts or protein, *Mastl*(ED/ED) knockin mice express normal levels of mutant mRNA (Figure S1A) or protein (Figure 1C) in platelets or megakaryocytes.

Mastl(Δ/Δ) and *Mastl*(ED/ED) mice were viable and fertile and displayed no overt abnormalities. The development of the hematopoietic system and their progenitors was normal in these models (Figure S1B). However, both mutant mice displayed reduced platelet counts in peripheral blood [~20% reduction in *Mastl*(Δ/Δ) and ~15% reduction in *Mastl*(ED/ED) mice] and a significant percentage of 8-12-week-old animals with reduced (<700 x 10^3 platelets/μl blood) counts of platelets (Figure 1D, E). Whereas thrombocytopenia was more obvious in *Mastl*(Δ/Δ) mice, the trend observed in young *Mastl*(ED/ED) was conserved in older (50-old) mice as well as in heterozygous

Mastl(+/ED) mutant mice (Figure S1C,D). Finally, although the mean volume of platelets was not affected in these mutants (Figure S1E), levels of TPO were slightly elevated in *Mastl*(Δ/Δ) and *Mastl*(ED/ED) mice (Figure 1F), suggesting the presence of physiological defects in platelet number or function.

To understand the cellular basis of these defects we next analyzed the maturation of megakaryocytes in vivo. *Mastl*(Δ/Δ) megakaryocytes in the bone-marrow displayed decreased expression of Von Villebrand Factor (VWF), a glycoprotein increasingly produced during maturation of these platelet-producing cells (Figure 1G). This defect however was not obvious in *Mastl*(ED/ED) mice. *Mastl*(Δ/Δ) mice also displayed reduced levels of fully-matured megakaryocytes (as scored by double CD41+ CD42+ staining) in the bone marrow (Figure 1H), although the ploidy of these cells was not affected (Figure 1I). *Mastl*(ED/ED) mutants, however, did not display defects in neither VWF expression, CD41/CD42 levels, nor ploidy (Figure 1G-I).

Altered platelet function in Mastl-null and Mastl E166D mice

Circulating platelet counts reflect the balance between platelet production and clearance. We therefore tested platelet function by submitting Mastl mutant mice to different assays. We first investigated circulating half-life of platelets by the administration of a Dylight 488-labeled anti-CD42c antibody. Both Mastl-deficient and Mastl E166D mice displayed a significant reduction in circulating half-life (Figure 2A), suggesting that increased clearance also contributes to the thrombocytopenia observed in Mastl-deficient mice, and may explain the defects in platelet counts in *Mastl*(ED/ED) mice. We did not find evidences for increased clearance of VWF-positive cells in liver sections (Figure S2A) or for protein desialylation using *Maackia amurensis* lectin (MAL1) or *Ricinus communis*

Agglutinin I (RCA-1) binding assays (Figure S2B). However, both *Mastl*(Δ/Δ) and *Mastl*(ED/ED) platelets displayed increased levels of Anexin V (Figure S2C), suggesting apoptosis as a potential mechanism to explain increase platelet clearance in these models. In agreement with reduced platelet counts, both *Mastl*(Δ/Δ) and *Mastl*(ED/ED) mice displayed increased bleeding time (Figure 2B) and defective clot retraction (Figure 2C).

We further evaluated the differences between these two models by inducing pulmonary embolism by intravenous injection of collagen and epinephrine. Lack of Mastl in the *Mastl*(Δ/Δ) model resulted in a significant protection of death in this model, in correlation with a reduced number of thrombi observed in the lungs (Figure 2D,E). Surprisingly, the presence of the Mastl E166D mutation resulted in the opposite phenotype: accelerated death accompanied by abundant and large thrombi in the lungs. In an independent model in which ferric chloride ($FeCl_3$) was used to induce vascular injury in the context of an aseptic closed vascular system, lack of Mastl resulted in slightly increased vessel patency, whereas Mastl E166D mice displayed accelerated vessel occlusion in the presence of large thrombi (Figure 2F,G). Although *Mastl*(Δ/Δ) mice displayed lower count of peripheral platelets than Mastl E166D mutants, the differences found in these in vivo assays suggest a fundamental difference in the defects caused by the lack of Mastl or the presence of the thrombocytopenia-associated mutation.

Functional defects in mutant platelet activation and spreading

To investigate the basis for the differences between the two Mastl mutant platelets, we tested the response of these cells to several stimuli. No significant differences were observed in the aggregation of *Mastl*(ED/ED) platelets in response to thrombin (Figure 3A,B) or collagen (data not shown), whereas Mastl-deficient platelets were significantly

inefficient in these assays. Exposure of isolated platelets to thrombin did not result in differences in the levels of high-affinity activated integrin αIIbβ3 (fibrinogen receptor or CD41a), suggesting no defects in the early inside-out pathway in mutant platelets (Figure 3C). However, whereas binding to fibrinogen was deficient in *Mastl*(Δ/Δ) platelets, it was enhanced in *Mastl*(ED/ED) mutant platelets perhaps suggesting a hyper-stabilization of fibrinogen-receptor complexes or deficient downstream events in the knockin model (Figure 3D). Both *Mastl*(Δ/Δ) and *Mastl*(ED/ED) platelets showed a defect in the generation of actin fibers after stimulation with fibrinogen when compared to control platelets, indicating defects in cytoskeletal dynamics in both models (Figure 3E). Fibrinogen uptake, a process that depends on endocytosis as well as re-organization of the actin cytoskeleton, was also deficient in *Mastl*(Δ/Δ) and *Mastl*(ED/ED) platelets, in line with the possible defects in outside-in signaling and/or cytoskeletal dynamics in these mutant cells (Figure 3F). All together, these data suggested cytoskeletal alterations in Mastl-mutant platelets, accompanied by deficient or enhanced signaling in *Mastl*(Δ/Δ) or *Mastl*(ED/ED) platelets, respectively.

To functionally validate the observed defects in cytoskeletal regulators, we next monitored the morphological changes during platelet activation using electron microscopy and fluorescence-guided studies. Resting *Mastl*(ED/ED) platelets were indistinguishable from control cells in their size or granule composition (Figure 4A). However, these mutant cells formed bigger aggregates after activation with thrombin and displayed a specific defect in the formation of lamellipodia, a structure typically formed of a dense and dynamic network of actin filaments (Figure 4B), in agreement with defects in actin cytoskeleton dynamics. We next monitored cytoskeletal changes during platelet activation by thrombin on fibrinogen-coated surfaces at different time points by

immunofluorescence. In resting conditions, platelets are characterized by the presence of a ring of microtubules and a diffuse actin staining. After thrombin activation, these cellular components are re-distributed to form tight rings of constricted microtubules and actin filaments thus favoring first the formation of filopodia and later lamellipodia characteristic of cell spreading (Figure 4C). In Mastl-deficient platelets, this process occurred with delayed kinetics. The presence of Mastl E166D, however, resulted in the rapid formation of long pseudopods with abundant microtubules after activation. The filaments of actin were not formed and platelets maintained these hyper-stabilized microtubule structures, ultimately leading to the formation of big aggregates at later time points (Figure 4C). As previously reported (21), this phenotype was reminiscent of that obtained after the inhibition of PP2A phosphatases in wild-type platelets (Figure 4D,E), suggesting that the Mastl E166D mutation may result in decreased PP2A activity.

Mastl E166D functions as a gain-of-function mutation

The MASTL E167D mutation was originally proposed as a loss-of-function mutation (14). However, the similarities between PP2A inhibition and the Mastl E166D mutation during platelet spreading suggests that this mutation may rather confer increased inhibitory activity to Mastl over PP2A. To understand the intrinsic effect of the E166D mutation we first performed kinase assays after transfection of exogenous cDNAs in human 293T cells. As indicated in Figure S3A, the activity of Mastl on substrates or its autophosphorylation decreases when using a standard kinase-dead mutation in this protein (D155A mutant). However, the thrombocytopenia-associated mutant (E166D) was not defective in this assay and resulted in slightly higher levels of both phosphorylation of myelin basic protein and autophosphorylation (Figure S3A). We also generated mouse embryonic fibroblasts (MEFs) carrying the E166D mutation in the

endogenous locus [*Mastl*(ED/ED]. As shown in Figure S3B, Mastl immunoprecipitates from *Mastl*(ED/ED) MEFs displayed slightly increase in MBP phosphorylation when compared to control samples.

Mastl is well characterized as a kinase required for the maintenance of the mitotic state by inhibiting mitotic PP2A-B55 complexes thus preventing the dephosphorylation of Cdk substrates (8, 9, 11, 12, 22). We therefore evaluated the relative functionality of the endogenous Mastl E166D mutant by testing its ability of supporting the mitotic state in dividing MEFs. As shown in Figure S3C, the presence of the Mastl E166D mutation resulted in increased phosphorylation of Cdk substrates (in agreement with reduced PP2A activity) after stimulation of quiescent cells with serum. These differences were not a consequence of differential progression through mitosis as determined with cyclin B1 and phosphorylation of histone H3. Similar results were obtained in cells arrested in mitosis with taxol and released after inhibiting Cdk1 to induce mitotic exit. The dephosphorylation of Cdk substrates was reduced in *Mastl*(ED/ED) MEFs, in agreement with reduced PP2A activity, despite a similar kinetics in the exit from mitosis as determined by the loss of cyclin B1 or histone H3 phosphorylation (Figure S3D). These assays were performed in the presence of taxol to increase mitotic entry due to the difficulties in synchronization of primary MEFs and no differences in the duration of mitosis were observed (Figure S3E), suggesting a specific alteration in the increased phosphorylation of substrates rather than differences in mitotic cells or the duration of mitosis.

Interestingly, the pattern of phosphorylation of MAPK-Cdk substrates (characterized by proline-directed phosphosites for which PP2A-B55 displays certain preference) was also inverted in Mastl-null versus Mastl E166D platelets (Figure 5A), confirming the data described in MEFs. All together, these assays indicate that the E166D

mutation does not prevent Mastl activity and, instead, may result in a functional gain-of-function, at least in the phosphorylation of putative PP2A-B55 phospho-substrates.

Differential phosphorylation of actin cytoskeleton proteins in Mastl E166D platelets

To gain further insights into the phosphorylation changes of mutant platelets we performed a phospho-proteomics analysis in resting or activated platelets at different time points after exposure to thrombin (Figure 5B). 82,525 out of 127,584 peptides identified were phosphorylated (83% enrichment) belonging to 1542 phospho-proteins. 4328 individual phospho-sites were precisely localized (Class I) in these proteins (Figure 5B and Supplementary Table 1).

In resting *Mastl*(ED/ED) platelets, 65 residues (in 61 proteins) were hyperphosphorylated [$\log_2$ Fold Change(FC) *Mastl*(ED/ED)/*Mastl*(+/+) > 0.75] when compared to control platelets, with an enrichment [False Discovery Rate (FDR)<0.005] in KEGG pathways related to membrane signaling, focal adhesion and cytoskeleton (Figure 5C and Supplementary Table 2). 104 residues (85 proteins) were hypophosphorylated [$\log_2$FC *Mastl*(ED/ED)/*Mastl*(+/+) < 0.75] in these mutant platelets with no specific KEGG pathway or GO biological process enriched in that set of proteins. A similar comparison in *Mastl*(Δ/Δ) vs. Mastl(+/+) platelets showed no enriched pathway in the hyperphosphorylated proteins whereas focal adhesion was enriched (FDR<0.001) among the hypophosphorylated proteins (Figure 5D and Supplementary Table 3).

The bulk of phosphorylations increased 3 min after activation with thrombin and decreased at later time points in all different genotypes (Figure S4A). The signaling pathways involved in actin cytoskeleton reorganization upon focal adhesion was further hyperphosphorylated in *Mastl*(ED/ED) versus *Mastl*(+/+) platelets (121 residues in 95

proteins hyperphosphorylated; log_2FC ED/WT>0.75) 3 min after the exposure to thrombin (Figure S4B), whereas no special pathway was enriched among the proteins hyperphosphorylated in *Mastl*(Δ/Δ) platelets (Figure S4B and Supplementary Table 4). Analysis of the hyperphosphorylated sequences in *Mastl*(ED/ED) resting platelets showed high frequency of CAMKII and PKA/PKC motifs with a smaller representation of [S/T]-P phospho-residues (Figure 5E), a sequence preferentially dephosphorylated by PP2A-B55 complexes (23). Three minutes after activation with thrombin, [S/T]-P phospho-residues were much enriched in activated *Mastl*(ED/ED) platelets compared to control cells (Figure 5E).

A combined analysis of sequences hyperphosphorylated in both resting and 3-min-activated platelets (42 phospho-residues in 43 proteins; log_2FC ED/WT>0.75) suggested that focal adhesion and actin cytoskeleton were the most significant pathways with hyperphosphorylated components in resting and activated Mastl E166D platelets (Figure S5 and Supplementary Table 5). At later time points (15 and 45 min in the presence of thrombin), several additional pathways such as chemokine signaling, endocytosis, MAPK signaling pathway or inositol phosphate metabolism were also deregulated (Supplementary Tables 6 and 7).

The results obtained in functional assays (Figures 2-4) and proteomic studies (Figure 5) suggested specific alteration of phospho-proteins, including those with proline-directed phosphosites, involved in outside-in signaling downstream of integrin αIIbβ3 and in actin re-organization. The catalytic subunit of PP2A is known to associate constitutively with the integrin αIIbβ3 preventing spontaneous outside-in signaling (24). Binding of fibrinogen to αIIbβ3 leads to decreased integrin-associated PP2A activity, thereby favoring the phosphorylation of downstream targets such as the

enabled/vasodilator-stimulated phosphoprotein (Vasp), a critical regulator whose dephosphorylation is required for the dismantling of filopodia in order to form the lamellipodia required for spreading (25, 26). In *Mastl*(ED/ED) platelets, these changes were accompanied by enhanced activation of critical regulatory kinases such as protein kinase C (Pkc), Src or Fak (Figure 6 and S6A). Activation of these pathways likely resulted in increased phosphorylation of Vasp in both S157 and S322, which are known to increase stress fiber and filopodia formation (27), as well as the regulatory light chain of myosin II (Mlc2), a reporter of active re-organization of the actomyosin cytoskeleton. Inhibition Pkcδ, Pka or Ampk, three upstream kinases activated by αIIbβ3 during outside-in signaling and involved in Vasp phosphorylation (25, 28, 29), prevented Vasp hyperphosphorylation and downstream events in *Mastl*(ED/ED) platelets (Figure 6). In addition, treatment of wild-type platelets with the PP2A inhibitors fostriecin (Figure 6) or okadaic acid (Figure S6B) resulted in hyperactivation of these signaling regulators to similar extent to that found in *Mastl*(ED/ED) platelets.

Functional relevance of altered actin dynamics in Mastl E166D platelets

The finding that actin regulatory networks are deregulated during the activation of *Mastl*(ED/ED) platelets prompted us to evaluate the possible relevance of actin deregulation in the phenotypes observed in these mutant mice. Treatment of platelets with cytochalasin D, a compound that prevents actin polymerization, resulted in a significant increase in the formation of long pseudopods with abundant microtubules, mimicking the aberrations observed in Mastl E166D mutant platelets (Figure 7A). On the other hand, cytochalasin D resulted in increased cell death in wild-type platelets but it did not enhance the increased cell death levels observed after the activation of *Mastl*(ED/ED) platelets (Figure 7B). Interestingly, this compound partially rescued the increased cell death

observed in Mastl-null platelets. Jasplakinolide, a compound that promotes actin polymerization and prevents its disassembly, resulted in different aberrations in wild-type platelets, characterized by aberrant lamellipodia (Figure 7A). Interestingly, jasplakinolide partially rescued cell death in Mastl E166D mutant platelets but did not have a significant effect in Mastl-null platelets (Figure 7B).

We next asked whether the abnormal behavior of *Mastl*(ED/ED) platelets could be rescued by inhibiting critical kinases upstream of Vasp and Mlc2 phosphorylation and actin cytoskeleton re-arrangements. Indeed, treatment of *Mastl*(ED/ED) platelets with Ampk, Pka and Pkc inhibitors rescued the formation of the abnormal pseudopod-like structures observed after thrombin-dependent activation of *Mastl*(ED/ED) platelets in a fibrinogen-coated surface (Figure 7C).

We finally tested the effect of these kinase and phosphatase inhibitors in blood coagulation in vivo, As shown in Figure 8A, PP2A inhibition enhanced thromboembolism formation in wild-type mice thereby mimicking the effect of the Mastl E166D mutation (compare to Figure 2D). On the other hand, treatment of *Mastl*(ED/ED) mice with Ampk, Pka and Pkc inhibitors delayed embolism formation (Figure 8B) as well as embolism-induced death (Figure 8C) in the presence of the thrombocytopenia-associated mutation. All together, these data suggest that Mastl E166D mutant platelets display an aberrant phosphorylation pattern that may contribute to defective platelet function and thrombocytopenia.

DISCUSSION

The Ser/Thr kinase Mastl has emerged as an essential module in the inhibition of cell cycle phosphatases, thus ensuring the maintenance of critical phospho-residues during

mitosis (1, 2). In the absence of Mastl, PP2A-B55 activity raises resulting in deficient phosphorylation of mitotic proteins. In yeast, Mastl homologues are involved in nutrient sensing or the regulation of transcription during quiescence or meiosis in a PP2A-dependent manner (30, 31). Whether Mastl plays any role in mammalian postmitotic cells remains unexplored.

The identification of a missense mutation in the human *MASTL* gene in patients with thrombocytopenia type II (THC2; MIM 188000) (14, 16) suggested a putative role for this kinase either during the endomitotic process in megakaryocytes or in platelet function. The mutation in *MASTL* (E167D) perfectly segregated with thrombocytopenia affected individuals and it was not present in unaffected family members of unrelated individuals. Subsequent studies in zebrafish indicated reduced thrombocyte levels upon Mastl knockdown (32) although these studies were performed using specific morpholinos to eliminate Mastl expression, and the relevance of the thrombocytopenia-associated point mutation remained unclear. Our data using conditional mouse models or a knockin expressing the E166D (homologous to E167D in humans) mutant suggest that, whereas Mastl deficiency leads to defective maturation in high-ploidy megakaryocytes, Mastl E166D megakaryocytes show no obvious alterations in these platelet precursors. *Mastl* ablation does not prevent mitotic entry in mammalian cells (12) and *Mastl*-null megakaryocytes are able to reach normal ploidy levels, probably reflecting the fact that proper chromosome condensation or segregation is not required for endomitosis, similarly to what reported in Aurora B-null megakaryocytes (33).

Interestingly, *Mastl*(ED/ED) mice display mild thrombocytopenia characterized by normal platelet size and volume, and increased levels of TPO, mimicking some of the characteristics of THC2 patients (16). THC2 patients are also characterized by other phenotypes not reproduced in Mastl E166D mice, such as defective polyploidy and

megakaryocyte differentiation (16), two phenotypes that are frequently attributed to specific nucleotide substitutions in the adjacent *ANKRD26* gene. In fact, THC2 is now considered to be mostly a consequence of monoallelic single nucleotide substitutions in the 5'-UTR of the *ANKRD26* gene (17, 18). These mutations lead to impaired binding of the transcription factors RUNX1 and FLI1 resulting in ANKRD26 overexpression, increased MAPK signaling and defective megakaryocyte maturation and proplatelet formation (34). Due to the frequency of these *ANKRD26* alterations and the fact that *ANKRD26* and *MASTL* are neighbor genes in the THC2 locus at human chromosome 10p11-12, it was unclear to what extent MASTL E167D was a passenger mutation or had any causal role in the development of this disease.

Our findings showing that Mastl E166D mice display mild thrombocytopenia and defective platelet activation not only indicate a causative role for Mastl mutations in thrombocytopenia, but also suggests for the first time a cell-cycle-independent role for this kinase in mammalian tissues. During the cell cycle, Mastl specifically inhibit PP2A phosphatase complexes containing B55 (B55α, β, γ, δ) regulatory subunits to counteract Cdk-dependent phosphorylation (8, 22). In platelets, PP2A counteracts major kinase pathways (PKC, CMK2, CK2)(21), associates with the cytoskeletal fraction under aggregating conditions (35), and regulates outside-in signaling with a significant effect in the focal adhesion pathway (36). PP2A is a critical inhibitor of the outside-in signaling pathway downstream αIIbβ3 and PP2A inhibition is known to enhance αIIbβ3 adhesion to fibrinogen and phosphorylation of downstream events (24). PP2A directly dephosphorylates critical signaling molecules during platelet activation, such as protein kinase C-zeta (PKCz)(37) or VASP (24, 38). Inhibition of PP2A leads to defective spreading after activation with thrombin resulting in cells with long pseudopods with hyperestabilized microtubules (21), similar to what observed in Mastl E166D platelets

(Figure 4). Inhibition of PP2A in interphasic cells is known to induce a similar phenotype resulting in short dynamic microtubules typical of mitosis (39), suggesting certain parallelism in the mechanism of action of PP2A in preventing hyper-stabilized microtubules both in platelet and pre-mitotic cells.

The exact mechanisms that regulate Mastl kinase activity are not well established. However, glutamine 166 is predicted to be close to the C-terminal tail required for activation of the kinase (40, 41), thus suggesting that the substitution of E by D may lead to different affinities for the activating tail. The common phenotypes induced by Mastl E166D and PP2A inhibition suggests that the E166D is not a loss-of-function mutation as originally suggested based on a similar mutation (E-to-D) in the tyrosine kinase Jak2 (E1046D) shown to abolish kinase activity (42). In fact, our data suggest that Mastl E166D may be a functional gain-of-function alteration based on a) increased phosphorylation of proline-directed sequences (frequently dephosphorylated by PP2A-B55 phosphatases) in fibroblasts (Figure S3) and platelets (Figure 5A), b) functional assays in fibroblasts (Figure S3), c) activation of signaling pathways (Figure 6), and d) the fact that PP2A inhibition mimics its effects in platelet spreading (Figure 4D,E) and a model of pulmonary embolism (Figure 8A). However, to what extent the defects observed in Mastl-mutant platelets are a direct consequence of differences in PP2A activity or are due to alterations in other putative Mastl substrates is unclear at the moment.

Overall, the analysis of the MASTL thrombocytopenia-associated mutation in platelets has uncovered a new function for MASTL in the regulation of actin dynamics in postmitotic cells. Given the relevance of MASTL in cancer therapy (43), whether this function also contributes to cytoskeletal dynamics in proliferating or tumor cells is an intriguing possibility that deserves further research. Our data suggest that the MASTL E167D mutation may contribute to thrombocytopenia by altering the dynamics of platelet

activation as a consequence of deregulated phosphorylation events affecting the outside-in pathway and actin cytoskeleton changes. The pathogenic effect of this mutation can be prevented by inhibiting critical outside-in kinases, an observation with putative implications for THC2 patients carrying this mutation.

METHODS

Generation of mutant mice

The conditional loss-of-function model of Mastl was generated by flanking exon 4 of the murine *Mastl* locus with loxP sites (Figure 1A) (12). These mice were crossed with Pf4-Cre transgenics (20) to generate megakaryocyte-specific loss of Mastl. The new thrombocytopenia knockin model was generated by replacing the wild-type allele with a mutant allele carrying the E166D mutation (Figure 1B), analog to the E167D mutation found in human thrombocytopenia. Recombinant ES cells harboring this allele were electroporated into developing morulas and the resulting mice were crossed with Actin-Flp transgenics to generate *Mastl*(+/E166D) mice. Mice were maintained in a CD1 x C57BL/6J x 129Sv/J mixed background. Mice were housed in the pathogen-free animal facility of the Centro Nacional de Investigaciones Oncológicas (CNIO, Madrid) following the animal care standards of the institution. These animals were observed on a daily basis and sick mice were killed humanely in accordance with the Guidelines for Humane End Points for Animals used in biomedical research.

For histological examination, samples were fixed in a solution of 4% of paraformaldehyde, embedded in paraffin and cut in 2.5-µm sections. Sections were then stained with hematoxylin and eosin (H&E) or Cartair's staining with the Carstais's stainig kit (Electron Microscopy Sciences, CatnNo26381-Series), following the manufacture's

protocol. For immunohistochemistry, a von Willebrand factor antibody (FVIII, Dako; 1:2000) was used. Sections were examined using a Nikon ECLIPSE 90i microscope using a CFI Plan Apo Lambda 4X/0.2 WB20 and a CFI Plan Apo Lambda 20X/0.75 DIC/N2 WB1.0, and processed using the ImageJ software. Further details in the antibodies used in this work are included in Supplementary Table 8.

Blood analysis

For platelet counts, blood sampling was performed from mandibular vein, collecting the blood into EDTA-coated tubes. Blood cell counts were assessed on an automated analyzer (Abacus Jr Vet, Vienna, Austria). Plasmatic TPO levels were measured with a Quantikine Mouse Thrombopoietin ELISA Kit (R&D Systems), following the manufacturer´s guidelines. Plasma from Cdc20-deficient mice (33), which display severe thrombocytopenia were included as a control.

Isolation and analysis of hematopoietic cells

Cells from the bone marrow or fetal liver were isolated as indicated in (33). The tibia and femur were isolated from 8-12-week old mice and bone marrow was flushed out by the addition of ice-cold PBS buffer (PBS, 0.5% BSA, 5 mM EDTA) through the lumen of the bone. Marrow was mechanically disrupted to achieve single cell suspension followed by filtering through a 40 μm nylon strainer to remove bone debris and subsequently subjected to erythrocyte lysis in ACK lysis buffer (150 mM ammonium chloride, 1 mM potassium bicarbonate, 0.1 mM EDTA; 90 s on ice). The lysis was stopped by the addition of 10 ml PBS buffer and cells were centrifuged at 200 g for 10 minutes. Cells were counted and subjected either directly to surface antigen staining for flow cytometry analysis or to lineage depletion with the MACS (magnetic cell sorting) Hematopoietic

Progenitor (Stem) Cell Enrichment Set (Miltenyi Biotec) according to manufacturer's protocol.

Megakaryocytes were isolated from bone marrow samples by staining with monoclonal allophycocyanin (APC)-CD41 antibody (BD Biosciences), followed by incubation with Anti-APC MicroBeads (Miltenyi Biotec). The cell suspension was then loaded onto a Large Cell separation MACS® Column and megakaryocytes were positive selected in a MACS Separator and columns (Miltenyi Biotec). For fetal liver derived megakaryocytes, cells were obtained from whole livers recovered from mouse fetuses between embryonic days 12.5 and 13.5. Single-cell suspensions were prepared by successive passage through 19-, 22-, and 25-gauge needles. Lin- cells were grown in Dulbecco's modified Eagle's medium (DMEM; GIBCO) supplemented with antibiotics and 10% fetal bovine serum (FBS), and stimulated with 50 ng/ml murine TPO (PeproTech) during at least 5 days. Ploidy of derived megakaryocytes was analysed at day 1, 3 and 5 of differentiation by staining with Fluorescein-5-isothiocyanate (FITC) anti-CD41 and 1 μg/ml of 4′,6-diamidino-2-phenylindole (DAPI; Sigma-Aldrich) in methanol-fixed derived megakaryocytes. Ten thousand-gate events were collected per experiment in a BD FACSCanto™ II cytometer (BD Biosciences). Data was analyzed using FlowJo Version 8.8.7 software (TreeStar).

To quantify bone marrow hematopoietic stem cells, freshly cells from the bone marrow were stained with phycoerythrin (PE) anti-CD34, Alexa Fluor 488 anti-IL7Ra, peridinin chlorophyll Protein Cyanin 5.5 (PerCP-Cy 5.5 anti–Sca-1, allophycocyanin-H7 (APC-H7) anti-cKit, phycoerythrin-cyanin 7 (PE-Cy7), anti-FcγR and APC-labeled lineage cell detection cocktail (all from BD Biosciences). To determine ploidy from bone marrow megakaryocytes, methanol-fixed bone marrow cells were stained with APC anti-CD42, FITC anti-CD41 and 1 μg/ml DAPI. In all assays, 10,000-gate events were

collected per sample in a BD FACSCanto™ II cytometer (BD Biosciences). Data were analyzed using FlowJo Version 8.8.7 software (TreeStar). The details of the antibodies used are listed in Supplementary Table 8.

Platelets were isolated as described previously described (44). Briefly, mice were anesthetized with ketamine (100 mg/kg) and xylacine (10 mg/kg), and whole blood was drawn from the inferior vena cava into a syringe containing acid citrate dextrose (1 volume of anticoagulant/9 volumes of blood). Blood was mixed with one volume of modified HEPES-Tyrode's buffer (140 mM NaCl, 2 mM KCl, 12 mM $NaHCO_3$, 0.3 mM NaH_2PO_4, 1 mM $MgCl_2$, 5.5 mM glucose, 5 mM HEPES, 2 mM EGTA and 0.035% BSA, pH 6.7) and it was centrifuged at 150 g for 2 min to obtain platelet-rich plasma (PRP). 5 nM of Prostaglandin E1 (PGE1; Sigma-Aldrich) was then added and platelets were pelleted by centrifugation at 1,500 g for 4 minutes at 37 °C. Platelet pellets were finally suspended in modified HEPES-Tyrode's buffer without EGTA and BSA (pH 7.38) but in the presence of 0.02 U/ml of Apyrase (Grade VII; Sigma-Aldrich). Platelets were counted and pooled at a density necessary for each experiment.

mRNA expression analysis

mRNA extraction from platelets was performed following the protocol described for the commercial reactive Trizol® (Invitrogene). RNA reverse transcription was performed with the High Capacity cDNA Reverse Transcription Kit (Applied Biosystems), using 500 ng of total RNA in each reaction and following the protocol described in the kit. *Mastl* mRNA levels were measured by real-time PCR using SYBR Green PCR Master Mix (Applied Biosystems). For amplification, primers placed in targeted region (*Mastl* exon 3/4) were used: forward, 5′-AGACTACCTGCACAGACATGGA-3′ and reverse, 5′-TTGGAAAGGCAAAATCTGTCAGT-3′; and *Gapdh*: forward, 5′-

TCAACAGCAACTCCCACTCTTCCA-3′ and reverse, 5′-ACCCTGTTGCTGTAGCCGTATTCA-3′. Amplification was performed in an Applied Biosystems 7900HT Fast Real-Time PCR System, using the following conditions: initial activation 50ºC for 20 s, initial denaturation at 95ºC for 600 s and 45 cycles of (95ºC for 15 s, 60ºC for 40 s, and 72ºC for 20 s), at transition rates of 4.8ºC/s, except for annealing which was 2ºC/s. The program for melting curve analysis was 95ºC for 10 s, 65ºC for 30 s with a 2.5ºC/s transition rate, and then ramping to 95ºC at a transition rate of 0.1ºC/s. Ct values were determined automatically and analyzed using the by the SDS Software 2.2. *Gapdh* mRNA levels were used as an internal control for normalization.

Analysis of platelet lifespan

To analyze platelet lifespan, mice were injected i.v. with 0.2 mg/kg of DyeLight488-labelled anti-CD42c (GPIbβ) antibody (Emfret Analytics, Germany). After 1 h, 10 μl of whole blood from maxillary vein was collected into EDTA-coated tubes. Whole blood was diluted (1/25) in PBS and the PRP was obtained by centrifugation at 1,500 g for 5 minutes. PRP was then stained with APC anti-CD41 (eBiosciences) and, after further dilution with PBS (1/2), samples were analyzed. Ten thousand $CD41^+$-gate events were collected per sample in a BD FACSCanto™ II cytometer (BD Biosciences). Data was analyzed using FlowJo Version 8.8.7 software (TreeStar) and results were expressed as percentage of $DyeLight^+$ events respect to the total of $CD41^+$ events. Platelet counts were obtained daily for 5 days at the same time.

Tail bleeding time and clot retraction

Tail bleeding time measurements were performed as described earlier (45), with some modifications. Mice were anesthetized with an i.p. injection of ketamine (100 mg/kg) and

xylazine (20 mg/kg). The tip of the tail was cut and immediately immersed in PBS pH 7.4 pre-warmed at 37°C. The mice and the pre-warmed tubes PBS were placed into an incubator at 37ºC for maintain them at the same temperature along the measurements. Bleeding time was defined as the time needed for the cessation of visible blood stream for two minutes. Monitoring of the bleeding times was stopped at 10 minutes by cauterizing the tails to prevent excessive loss of blood.

Clot retraction assays were performed as previously described (46). Washed platelets were counted and adjusted to $5x10^8$ platelets/mL with Hepes Tyrode's Buffer supplemented with 2 mM $MgCl_2$, 2 mM $CaCl_2$ and 2 mg/mL fibrinogen (Sigma-Aldrich). Clot retraction assays were performed at 37 ºC without stirring, in siliconized glass cuvettes with 400 µL of platelet suspension in the presence of 10 IU/mL of thrombin (Chrono-log Corp). Clots were monitored every 15 min up to 120 min after clot induction. The area of the clot was analyzed in each picture by Image J software (http://rsb.info.nih.gov/ij/). At the final time point, the clot exudate was collected and the wet clot weighed.

Ferric chloride ($FeCl_3$)-induced carotid artery injury

These studies were performed essentially as reported previously (47, 48). Mice were anesthetized with isoflurane (Abbott Laboratories) and the left carotid artery was exposed. A 0.5-1.0-mm strip of Whatman No. 1 filter paper soaked in 5% $FeCl_3$ solution was applied to the surface of the adventitia for 3 min. Carotid blood flow was monitored with a miniature ultrasound flow probe (0.5VB, Transonic Systems) interfaced with a flowmeter (model T106, Transonic Systems) and a computerized data acquisition program (WinDaq, DATAQ Instruments). At the end of the 30-min flow-monitoring

period, mice were euthanized by cervical dislocation and the carotid artery was excised for histological purposes.

Collagen/epinephrine-induced pulmonary thromboembolism

To induce thromboembolism, mice were anesthetized as described in tail bleeding assays and a mixture of 0.5 mg/kg of equine collagen (Hormon Chemie, München, Germany) and 60 μg/kg of epinephrine (Sigma) was injected into the jugular vein. Most mice died within the first 15 min; otherwise, they were euthanized by cervical dislocation. Histological examination of the lungs was performed to determine whether vessels of the microcirculation were occluded by thrombi consisting of platelet aggregates formed in response to the epinephrine-collagen. When indicated, mice were treated with kinase or phosphatase inhibitors for 1 h before of the induction of pulmonary embolism. These drugs were administered by i.v. injection at the following doses: 0.5 mg/kg Fostriecin, 0.2 mg/kg Dorsomorphin 2-HCl (Compound C analog), 1 mg/kg H89, 10 mg/kg Gö6983, 0.5% DMSO or vehicle (10% PEG400; 0.16% Tween80; 1.6% propylene glycol).

In vitro aggregation studies

For aggregation studies of murine platelets, 500 μl of washed platelets at $5x10^8$ platelet/ml were used. Optical platelet aggregation experiments were monitored by a turbidimetric method using an aggregometer (Chronolog 490 optical aggregometer) with continuous stirring at 1200 rpm at 37°C. A final concentration of 0.5 UI/ml of Thrombin and 5 μg/ml of collagen (Cronolog Corp.) were used as agonists for aggregation studies.

Platelet Flow Cytometry assays

To determine integrin αIIbβ3 (GPIIb/IIIa) activation in mice platelets, 100 µl of $1x10^6$ platelets/mL of washed platelets were incubated for 15 min at RT with rat anti-mouse-PE-CD41a (JON/A) alone (resting) o together 0.05 IU/mL of thrombin (activated). Reactions were stopped by addition of 400 µl PBS and samples were analyzed within 30 minutes by FACS. The mean fluorescence intensity of mutant versus wild-type platelets was used to measure the activated conformation of mouse integrin αIIbβ3 (GPIIb/IIIa, CD41/CD61).

Ex-vivo Fibrinogen binding (Fg-binding) and Fibrinogen Uptake (Fg-uptake) assays were performed following the protocol described previously (49) with minor modifications. Basically, 100 µl of $1x10^7$ platelets/mL of washed platelets were supplemented with 0.15 mg/mL AlexaFluor^{TM}488-conjugated human fibrinogen (Molecular Probes) and 2mM $CaCl_2$. Platelets were then incubated for 30 minutes at 37 ºC, fixed with 2% paraformaldehyde and analyzed by flow cytometry. To study Fg-uptake, washed platelets (100 µl of $1x10^7$ platelets/mL) were incubated with Fg-AlexaFluor^{TM}488 (0.15 mg/mL) at 37°C for 30 minutes. Platelets were fixed with 2% paraformaldehyde and, after addition of 0.04% trypan blue, analyzed by flow cytometry.

For determination of intracellular F-actin levels, 100 µl of $1x10^7$ platelets/mL were incubated with 0.05 IU/mL of thrombin for 3 and 15 min prior to fixation with with 2% paraformaldehyde. Platelets were then permeabilized with 0.05% Triton X-100 and stained using 2 mM AlexaFluor^{TM}488-phalloidin for 1h at RT. Platelets were washed twice with PBS and then analyzed by flow cytometry.

Platelet surface sialylation and galactose exposure was analyzed by incubation of 100 µl of washed platelets ($1x10^7$ platelets/mL) with rat anti-mouse-PECy7-CD41 and fluorescein-labelled Ricinus Communis Agglutinin I (FL-RCA I, used at final concentration of 0.5 µg/ml) or fluorescein-labelled Maackia Amurensis Lectin I (FL-

MAL I, used at final concentration of 0.5 µg/ml)(Vector Laboratories) for 45 min at RT. Platelets were washed with PBS twice and analyzed by flow cytometry.

For annexin V staining, ten million of platelets were suspended in 100 µl of 1X Binding Buffer (0.01 M HEPES, pH 7.4; 0.14 M NaCl; 2.5 mM $CaCl_2$) and incubated for 1, 3 or 6 hours at 37 ºC. When indicated, platelets were also incubated in the presence of 10 µM of Cytochalasin D (Sigma-Aldrich) or 5 µM of Jasplakinolide (Tocris). Staining was performed adding 5 µl of APC-AnnexinV (BD Bioscience) and 1µl of FITC-CD41 [MWReg30] or FITC-CD9 [EM-04] (BD Bioscience) for 30 min at RT. Reaction was stopped by adding 400 µl of 1X Binding Buffer and it was immediately analyzed by flow cytometry.

In all assays described above, 10,000 platelet-gate events were collected per experiment in a BD FACSCanto™ II cytometer (BD Biosciences). Data were analyzed using FlowJo Version 8.8.7 software (TreeStar) and MFI was use to evaluate Fg-binding, Fg-uptake, F-actin content, sialylation and Annexin V binding, respectively.

Transmission electron microscopy

Resting and thrombin (0.05 IU/mL, 15 min) activated platelets were fixed for 3 h at RT in 3% glutaraldehyde (vol/vol) in 0.4 M N-2-hydroxyethylpiperazine-N'-2-ethanesulfonic acid buffer pH 7.4, washed and fixed again in aqueous 1% (wt/vol) osmium tetroxide, and embedded in Epon. Electron microscopy was performed with a JEOL 1230 transmission electron microscope, at 80 kV, on ultrathin sections of 60 nm Biochemical assays.

Analysis of mouse embryonic fibroblasts

Mouse embryonic fibroblasts were isolated from E13.5 embryos and analyzed using routine cell cycle protocols (12). For flow cytometry analysis, cells were washed in PBS and fixed in ice-cold 70% ethanol. For identification of mitotic cells, cells were blocked using 3% bovine serum albumin (BSA) in PBS for 1 h followed by addition of MPM2 antibody (Millipore, 1:200) in blocking solution. Antibodies were detected with AlexaFluor 594 (1:1000) and DAPI was used to stain nuclei. Cell cycle profiles were determined by FACSCanto II flow cytometry system (BD Biosciences). The data were analyzed with the FlowJo software v7.5.

Biochemical assays

Two hundred and fifty microliters of washed platelets at 5×10^8 platelets/ml were supplemented 0.05 IU/ml of Thrombin (Cronolog cop.) and incubated at 37 ºC for different times. Then, 250 µl of 2X RIPA lysis buffer (100 mM Tris-HCl pH 8.0; 0.2% SDS, 2% NP-40, 1% sodium deoxycholate) supplemented with a mixture of protease and phosphatase inhibitors (PhosSTOP and Complete Protease Inhibitor Cocktail, Roche Applied Science) were added. The homogenate was incubated in ice for 30 minutes and centrifuged at 13,000 g for 15 minutes at 4 ºC, collecting the supernatant. Protein lysates from MEFs were prepared as described previously (11). Total protein was quantified using a selective colorimetric detection by bicinchoninic acid commercial kit (BCA Protein Assay Reagent Kit, Pierce) and samples were boiled in Loading buffer (70% (v/v) 0.5M Tris-HCl-0.4% (w/v) sodium dodecil sulphate pH 6.8, 30% (v/v) glycerol, 10% (w/v) SDS, 9.3% (w/v) dithioteitol, 0.012% (w/v) bromophenol blue and 10% (v/v) β-mercaptoethanol) at 98 ºC for 10 minutes.

For western blot analyses, 50 µg of total protein extract from murine platelets were analyzed by SDS-PAGE (4–15% Criterion™ TGX™ Precast Midi Protein Gel) before transfer to a nitrocellulose membrane. Membranes were blocked for 1 h at room temperature with 5% (w/v) of non-fatty milk in TBS-T (50 mM Tris-Cl, 100 mM NaCl, 0.1% Tween-20, pH 7.4) and incubated overnight at 4 ºC with the indicated antibodies (Supplementary Table 8). All membranes were rinsed 3 times with TBS-T and incubated with secondary antibodies conjugated with HPR. Protein detection was done using the ECL Advance Western Blotting Detection System (Amersham Biosciences) and X-ray fim exposure, following the recommendations of the manufacturer.

For in vitro kinase assays, HEK293 cells (ATCC) were transiently transfected with the indicated V5-tagged Mastl mutants. Cells were lysed in ELB buffer (50mM Hepes pH 7.5, 150 mM NaCl, 5mM EDTA, 1% NP-40) in the presence of protease and phosphatase inhibitors. Exogenous Mastl was immunoprecipitated with an anti-V5 antibody (Invitrogen), and immunocomplexes were incubated in kinase buffer (20mM Hepes pH 7.5, 10 mM MgCl2, 1 mM DTT) in the presence of 50 µM ATP, 2 µCi 32P-γ-ATP and 2 µg of myelin basic protein (MBP) as a substrate, during 30 min at 30ºC. Samples were analysed by SDS-PAGE, transferred to a nitrocellulose membrane, and images were obtained by autoradiography. Quantifications were performed using a Phosphorimager. For measuring the activity of Mastl in MEFs, cells were lysed in ELB buffer and endogenous Mastl was immunoprecipitated with an anti-Mastl antibody (Abgent). Kinase assays were performed following the same protocol as described above.

Uncropped scans of all gels shown in the manuscript are included in Figure S7.

Phospho-proteomics analysis

Cells were lysed using 7 M urea, 2 M thiourea, in 100 mM Hepes pH 7.5, supplemented with 1:1000 (v/v) of benzonase (Novagen) and 1:100 (v/v) of HaltTM phosphatase and protease inhibitor cocktail 100x (Thermo Fisher Scientific). Protein concentration was determined using the Pierce® 660nm Protein Assay (Bio-Rad) using BSA as standard. Then, samples (160 µg) were digested by means of the standard FASP protocol. Briefly, proteins were reduced (15 mM TCEP, 30 min, room-temperature), alkylated (50 mM CAA, 20 min in the dark, room-temperature) and sequentially digested with Lys-C (Wako) (protein:enzyme ratio 1:50, o/n at room-temperature) and trypsin (Promega) (protein:enzyme ratio 1:100, 6 h at 37 °C). Samples were labeled using iTRAQ® reagent 8-plex following manufacturer's instructions. Samples were mixed in 1:1 ratios based on total peptide amount, which was determined from an aliquot by comparing overall signal intensities on a regular LC-MS/MS run. The final mixture was finally desalted using a Sep-Pak C18 cartridge (Waters) and dried.

Phosphopeptides were enriched using home-made TiO_2 micro-columns. Briefly, peptides were resuspended in 6% TFA and 80% CH_3CN and incubated for 20 min with TiO_2 beads (10 µm particle size) (GL-Science) using a sample:TiO_2 ratio of 1:2. Prior incubation, TiO2 beads were pre-conditioned with a solution of 20 mg/mL DHB in 80% CH_3CN 6% TFA for 20 min. Then, beads were sequentially washed with 100 µL of 6% TFA and 10% CH_3CN, 100 µL of 6% TFA and 100 µL of 40% CH_3CN and 6% TFA and 60% CH_3CN. Finally, phosphopeptides were eluted first with 20 µL of 5% NH_4OH and then with 20 µL 5% NH_4OH in 10% CH_3CN in the same vial.

Phosphopeptides were fractionated offline by means of a high pH reverse phase micro-column. Samples were dissolved in phase A (20 mM NH_4OH) and loaded into a tip containing 5 discs of C18 and the flow-through was collected to a vial. Peptides were

sequentially eluted by increasing the percentage of buffer B (20 mM NH_3 in CH_3CN) (i.e. 4, 8, 12, 20, 60 and 80%). Last three fractions were pooled together.

LC-MS/MS was done by coupling a nanoLC-Ultra 1D+ system (Eksigent) to an Impact mass spectrometer (Bruker) via a Captivespray source (Bruker) supplemented with a nanoBooster operated at 0.2 bar/min with isopropanol as dopant. Peptides were loaded into a trap column (NS-MP-10 BioSphere C18 5 µm, 20 mm length, Nanoseparations) for 10 min at a flow rate of 2.5 µl/min in 0.1% FA. Then peptides were transferred to an analytical column (ReproSil Pur C18-AQ 2.4 µm, 500 mm length and 0.075 mm ID) and separated using a 95 min gradient (buffer A: 4% ACN, 0.1% FA; buffer B: 100% ACN, 0.1% FA) at a flow rate of 250 nL/min. The gradient used was: 0-2 min 6 % B, 2-80 min 30% B, 80.5-87.5 min 98% B, 88-95 min 2% B. The peptides were electrosprayed (1.35 kV) into the mass spectrometer with a heated capillary temperature of 180°C. The mass spectrometer was operated in a data-dependent mode, with an automatic switch between MS (80-1600 m/z) and MS/MS (80-1600 m/z) scans using a top 30 method (threshold signal $\geq$ 500 counts, $z \geq 2$ and $m/z \geq 350$). An active exclusion of 30 s was used. The precursor intensities were re-evaluated in the MS scan (n) regarding their values in the previous MS scan (n-1). Any m/z intensity exceeding 5 times the measured value in the preceding MS scan was reconsidered for MS/MS. Peptides were isolated using a 2 Th window and fragmented using collision induced dissociation (CID) with a collision energy of 23-56 eV as function of the m/z value.

For data analysis, raw files were processed with MaxQuant (v 1.5.8.3) using the standard settings against a mouse protein database (UniProtKB/Swiss-Prot and TrEMBL, August 2016, 43,965 sequences) supplemented with contaminants. Carbamidomethylation of cysteines was set as a fixed modification whereas oxidation of methionines, protein N-term acetylation and phosphorylation of serines, threonines and

tyrosines as variable modifications. Minimal peptide length was set to 7 amino acids and a maximum of two tryptic missed-cleavages were allowed. Results were filtered at 0.01 FDR (peptide and protein level). For phosphoproteome, the "phospho(STY)sites.txt" file was loaded in Perseus (v1.5.1.6) for further analysis. Phosphosites with a probability > 0.75 and a score difference < 5 were considered as localized (Class I). Phosphosites with a log_2FC ratio >0.75 or < -0.75 were considered as regulated. Over-representation of functional terms was performed with StringDB (50) using as background data set the platelets proteome (51) as background. A Fisher's exact test with multiple test correction was used and only terms with an FDR below 5% were considered as statistically significant.

The mass spectrometry proteomics data have been deposited to the ProteomeXchange Consortium via the PRIDE partner repository with the dataset identifier PXD009398.

Platelet Spreading assays

Spreading assays were performed as described previously (46). In brief, Lab-Tek™ Chamber Slides (Nunc) were coated overnight at 4ºC with 100 µg/ml of human fibrinogen (Sigma-Aldrich) in PBS, pH 8.0. Then, they were washed with PBS and blocked with 5 mg/ml of heat-denatured BSA for 2 h at RT, and then washed again. Platelets at $1x10^8$ platelets/mL were incubated on the fibrinogen coated chambers and let to spread for 5, 15, 30, and 60 min at 37ºC in presence of 0.05 IU/mL of thrombin. For actin inhibitors, platelets were allowed to adhere for 5 minutes and then, Cytochalasin D or Jasplakalodine were added at a final concentration of 10 µM and 5 µM, respectively, and let to spread for 15 minutes. After that, chambers were washed and adhered platelets were fixed with 4% of paraformaldehyde (PFA) for 10 min. After washing, chambers were incubated with

100 mM Glycine for 5 minutes and washed. Then, adhered platelets were permeabilized with 0.2% Triton X-100 for 5 min, washed and blocked with 10% normal goat serum (Sigma-Aldrich) for 30 min. Platelets were incubated with anti-α-tubulin primary antibody, followed by secondary antibody AlexaFluor488 goat anti-mouse. AlexaFluor564-Phalloidin was used to stain F-actin. Images were acquired with a Leica TCS SP5 WLL confocal laser microscope using a HCX PLAN APO CS 63x/1.4 Oil Immersion or HCX PLAN APO CS 100x/1.4 Oil Immersion. For platelet morphology quantification, at least 150 platelets per sample were measured using Fiji software.

Statistical Analysis

Statistical analyses were performed using Prism software (GraphPad Software). Unless stated otherwise, all statistical tests of comparative data were done using Mann-Withney test or two-sided, unpaired Student's t tests when Welch's correction when needed. For survival analysis, Log-rank (Mantel-Cox) Test with Bonferroni correction was applied. Data were expressed as means of at least three independent experiments ± SEM, with $P < 0.05$ considered statistically significant.

Study approval

All animal protocols were approved by the Instituto de Salud Carlos III/Comunidad de Madrid (Madrid, Spain) committee for animal care and research.

AUTHOR CONTRIBUTIONS

B.H. performed most platelet assays in vitro and in vivo with the help of A.E.B. M.T. generated the mouse models, contributed to some platelet assays, and characterized hematopoietic tissues and megakaryocytes with the help of D.P. and M.Maroto. R.S.-M. contributed to the generation of the knockin model. B.S. and M.T. performed the assays in MEFs, with the help of M.A.F. P.X-E and J.M. performed the phosphoproteomic analyses. L.M. helped with cytometry studies. P.G.dF. supervised the thrombosis models and contributed to the analysis of data. M. Malumbres designed and supervised the project, and wrote the manuscript with the help of B.H. and M.T.

ACKNOWLEDGEMENTS

We thank Peter Storz (Mayo Clinic; Jacksonville, FL) for sharing reagents and Sheila Rueda for her support with the management of the mouse colony. B.H. and R.S.-M. were supported by the Juan de la Cierva Programme from the Spanish Ministry of Economy and Competitiveness (MINECO). M.T. was supported by Foundation La Caixa. A.E.B. was supported by the Programa de Empleo Juvenil, Comunidad de Madrid. M.A.-F. received a young investigator grant from MINECO (SAF2014-60442-JIN; co-financed by FEDER funds). P.G.dF. was supported by Fundació la Marató de TV3 (project 080121 and project 20153031). J.M. was supported by the Ramon y Cajal programme (MINECO; RYC-2012-10651). M.M. lab. is supported by grants from the MINECO (SAF2015-69920-R), Programa iLUNG from the Comunidad de Madrid (B2017/BMD-3884), and Worldwide Cancer Research (15-0278). CNIO is a Severo Ochoa Center of Excellence (MINECO awards SEV-2015-0510).

REFERENCES

1. Glover DM. The overlooked greatwall: a new perspective on mitotic control. *Open Biol.* 2012;2(3):120023.
2. Lorca T, and Castro A. The Greatwall kinase: a new pathway in the control of the cell cycle. *Oncogene.* 2013;32(5):537-43.
3. White-Cooper H, Carmena M, Gonzalez C, and Glover DM. Mutations in new cell cycle genes that fail to complement a multiply mutant third chromosome of Drosophila. *Genetics.* 1996;144(3):1097-111.
4. Yu J, Fleming SL, Williams B, Williams EV, Li Z, Somma P, et al. Greatwall kinase: a nuclear protein required for proper chromosome condensation and mitotic progression in Drosophila. *J Cell Biol.* 2004;164(4):487-92.
5. Archambault V, Zhao X, White-Cooper H, Carpenter AT, and Glover DM. Mutations in Drosophila Greatwall/Scant reveal its roles in mitosis and meiosis and interdependence with Polo kinase. *PLoS Genet.* 2007;3(11):e200.
6. Gharbi-Ayachi A, Labbe JC, Burgess A, Vigneron S, Strub JM, Brioudes E, et al. The substrate of Greatwall kinase, Arpp19, controls mitosis by inhibiting protein phosphatase 2A. *Science.* 2010;330(6011):1673-7.
7. Mochida S, Maslen SL, Skehel M, and Hunt T. Greatwall phosphorylates an inhibitor of protein phosphatase 2A that is essential for mitosis. *Science.* 2010;330(6011):1670-3.
8. Vigneron S, Brioudes E, Burgess A, Labbe JC, Lorca T, and Castro A. Greatwall maintains mitosis through regulation of PP2A. *EMBO J.* 2009;28(18):2786-93.
9. Burgess A, Vigneron S, Brioudes E, Labbe JC, Lorca T, and Castro A. Loss of human Greatwall results in G2 arrest and multiple mitotic defects due to deregulation of the cyclin B-Cdc2/PP2A balance. *Proc Natl Acad Sci U S A.* 2010;107(28):12564-9.
10. Voets E, and Wolthuis RM. MASTL is the human orthologue of Greatwall kinase that facilitates mitotic entry, anaphase and cytokinesis. *Cell Cycle.* 2010;9(17):3591-601.
11. Manchado E, Guillamot M, de Carcer G, Eguren M, Trickey M, Garcia-Higuera I, et al. Targeting mitotic exit leads to tumor regression in vivo: Modulation by Cdk1, Mastl, and the PP2A/B55alpha,delta phosphatase. *Cancer Cell.* 2010;18(6):641-54.
12. Alvarez-Fernandez M, Sanchez-Martinez R, Sanz-Castillo B, Gan PP, Sanz-Flores M, Trakala M, et al. Greatwall is essential to prevent mitotic collapse after nuclear envelope breakdown in mammals. *Proc Natl Acad Sci U S A.* 2013;110(43):17374-9.
13. Alvarez-Fernandez M, and Malumbres M. Preparing a cell for nuclear envelope breakdown: Spatio-temporal control of phosphorylation during mitotic entry. *BioEssays.* 2014;36(8):757-65.
14. Gandhi MJ, Cummings CL, and Drachman JG. FLJ14813 missense mutation: a candidate for autosomal dominant thrombocytopenia on human chromosome 10. *Hum Hered.* 2003;55(1):66-70.
15. Bithell TC, Didisheim P, Cartwright GE, and Wintrobe MM. Thrombocytopenia Inherited as an Autosomal Dominant Trait. *Blood.* 1965;25:231-40.

16. Drachman JG, Jarvik GP, and Mehaffey MG. Autosomal dominant thrombocytopenia: incomplete megakaryocyte differentiation and linkage to human chromosome 10. *Blood.* 2000;96(1):118-25.
17. Pippucci T, Savoia A, Perrotta S, Pujol-Moix N, Noris P, Castegnaro G, et al. Mutations in the 5' UTR of ANKRD26, the ankirin repeat domain 26 gene, cause an autosomal-dominant form of inherited thrombocytopenia, THC2. *Am J Hum Genet.* 2011;88(1):115-20.
18. Noris P, Perrotta S, Seri M, Pecci A, Gnan C, Loffredo G, et al. Mutations in ANKRD26 are responsible for a frequent form of inherited thrombocytopenia: analysis of 78 patients from 21 families. *Blood.* 2011;117(24):6673-80.
19. Di Paola J, and Johnson J. Thrombocytopenias due to gray platelet syndrome or THC2 mutations. *Semin Thromb Hemost.* 2011;37(6):690-7.
20. Tiedt R, Schomber T, Hao-Shen H, and Skoda RC. Pf4-Cre transgenic mice allow the generation of lineage-restricted gene knockouts for studying megakaryocyte and platelet function in vivo. *Blood.* 2007;109(4):1503-6.
21. Yano Y, Sakon M, Kambayashi J, Kawasaki T, Senda T, Tanaka K, et al. Cytoskeletal reorganization of human platelets induced by the protein phosphatase 1/2 A inhibitors okadaic acid and calyculin A. *Biochem J.* 1995;307 (Pt 2):439-49.
22. Castilho PV, Williams BC, Mochida S, Zhao Y, and Goldberg ML. The M phase kinase Greatwall (Gwl) promotes inactivation of PP2A/B55delta, a phosphatase directed against CDK phosphosites. *Mol Biol Cell.* 2009;20(22):4777-89.
23. Rogers S, McCloy R, Watkins DN, and Burgess A. Mechanisms regulating phosphatase specificity and the removal of individual phosphorylation sites during mitotic exit. *BioEssays.* 2016;38 Suppl 1:S24-32.
24. Gushiken FC, Patel V, Liu Y, Pradhan S, Bergeron AL, Peng Y, et al. Protein phosphatase 2A negatively regulates integrin alpha(IIb)beta(3) signaling. *J Biol Chem.* 2008;283(19):12862-9.
25. Pula G, Schuh K, Nakayama K, Nakayama KI, Walter U, and Poole AW. PKCdelta regulates collagen-induced platelet aggregation through inhibition of VASP-mediated filopodia formation. *Blood.* 2006;108(13):4035-44.
26. Wentworth JK, Pula G, and Poole AW. Vasodilator-stimulated phosphoprotein (VASP) is phosphorylated on Ser157 by protein kinase C-dependent and -independent mechanisms in thrombin-stimulated human platelets. *Biochem J.* 2006;393(Pt 2):555-64.
27. Doppler H, and Storz P. Regulation of VASP by phosphorylation: consequences for cell migration. *Cell adhesion & migration.* 2013;7(6):482-6.
28. Butt E, Abel K, Krieger M, Palm D, Hoppe V, Hoppe J, et al. cAMP- and cGMP-dependent protein kinase phosphorylation sites of the focal adhesion vasodilator-stimulated phosphoprotein (VASP) in vitro and in intact human platelets. *J Biol Chem.* 1994;269(20):14509-17.
29. Onselaer MB, Oury C, Hunter RW, Eeckhoudt S, Barile N, Lecut C, et al. The Ca(2+) /calmodulin-dependent kinase kinase beta-AMP-activated protein kinase-alpha1 pathway regulates phosphorylation of cytoskeletal targets in thrombin-stimulated human platelets. *J Thromb Haemost.* 2014;12(6):973-86.
30. Chica N, Rozalen AE, Perez-Hidalgo L, Rubio A, Novak B, and Moreno S. Nutritional Control of Cell Size by the Greatwall-Endosulfine-PP2A.B55 Pathway. *Curr Biol.* 2016;26(3):319-30.

31. Moreno-Torres M, Jaquenoud M, and De Virgilio C. TORC1 controls G1-S cell cycle transition in yeast via Mpk1 and the greatwall kinase pathway. *Nat Commun.* 2015;6:8256.
32. Johnson HJ, Gandhi MJ, Shafizadeh E, Langer NB, Pierce EL, Paw BH, et al. In vivo inactivation of MASTL kinase results in thrombocytopenia. *Exp Hematol.* 2009;37(8):901-8.
33. Trakala M, Rodriguez-Acebes S, Maroto M, Symonds CE, Santamaria D, Ortega S, et al. Functional reprogramming of polyploidization in megakaryocytes. *Dev Cell.* 2015;32(2):155-67.
34. Bluteau D, Balduini A, Balayn N, Currao M, Nurden P, Deswarte C, et al. Thrombocytopenia-associated mutations in the ANKRD26 regulatory region induce MAPK hyperactivation. *J Clin Invest.* 2014;124(2):580-91.
35. Toyoda H, Nakai K, Omay SB, Shima H, Nagao M, Shiku H, et al. Differential association of protein Ser/Thr phosphatase types 1 and 2A with the cytoskeleton upon platelet activation. *Thromb Haemost.* 1996;76(6):1053-62.
36. Moscardo A, Santos MT, Latorre A, Madrid I, and Valles J. Serine/threonine phosphatases regulate platelet alphaIIbbeta3 integrin receptor outside-in signaling mechanisms and clot retraction. *Life Sci.* 2013;93(20):707-13.
37. Mayanglambam A, Bhavanasi D, Vijayan KV, and Kunapuli SP. Differential dephosphorylation of the protein kinase C-zeta (PKCzeta) in an integrin alphaIIbbeta3-dependent manner in platelets. *Biochem Pharmacol.* 2011;82(5):505-13.
38. Abel K, Mieskes G, and Walter U. Dephosphorylation of the focal adhesion protein VASP in vitro and in intact human platelets. *FEBS Lett.* 1995;370(3):184-8.
39. Tournebize R, Andersen SS, Verde F, Doree M, Karsenti E, and Hyman AA. Distinct roles of PP1 and PP2A-like phosphatases in control of microtubule dynamics during mitosis. *EMBO J.* 1997;16(18):5537-49.
40. Vigneron S, Gharbi-Ayachi A, Raymond AA, Burgess A, Labbe JC, Labesse G, et al. Characterization of the mechanisms controlling Greatwall activity. *Mol Cell Biol.* 2011;31(11):2262-75.
41. Blake-Hodek KA, Williams BC, Zhao Y, Castilho PV, Chen W, Mao Y, et al. Determinants for activation of the atypical AGC kinase Greatwall during M phase entry. *Mol Cell Biol.* 2012;32(8):1337-53.
42. VonDerLinden D, Ma X, Sandberg EM, Gernert K, Bernstein KE, and Sayeski PP. Mutation of glutamic acid residue 1046 abolishes Jak2 tyrosine kinase activity. *Mol Cell Biochem.* 2002;241(1-2):87-94.
43. Alvarez-Fernandez M, Sanz-Flores M, Sanz-Castillo B, Salazar-Roa M, Partida D, Zapatero-Solana E, et al. Therapeutic relevance of the PP2A-B55 inhibitory kinase MASTL/Greatwall in breast cancer. *Cell Death Differ.* 2018;25(5):828-40.
44. Cazenave JP, Ohlmann P, Cassel D, Eckly A, Hechler B, and Gachet C. Preparation of washed platelet suspensions from human and rodent blood. *Methods Mol Biol.* 2004;272:13-28.
45. Akbar H, Shang X, Perveen R, Berryman M, Funk K, Johnson JF, et al. Gene targeting implicates Cdc42 GTPase in GPVI and non-GPVI mediated platelet filopodia formation, secretion and aggregation. *PLoS One.* 2011;6(7):e22117.
46. Prevost N, Kato H, Bodin L, and Shattil SJ. Platelet integrin adhesive functions and signaling. *Methods Enzymol.* 2007;426:103-15.

47. Farrehi PM, Ozaki CK, Carmeliet P, and Fay WP. Regulation of arterial thrombolysis by plasminogen activator inhibitor-1 in mice. *Circulation.* 1998;97(10):1002-8.
48. Konstantinides S, Schafer K, Thinnes T, and Loskutoff DJ. Plasminogen activator inhibitor-1 and its cofactor vitronectin stabilize arterial thrombi after vascular injury in mice. *Circulation.* 2001;103(4):576-83.
49. Huang Y, Joshi S, Xiang B, Kanaho Y, Li Z, Bouchard BA, et al. Arf6 controls platelet spreading and clot retraction via integrin alphaIIbbeta3 trafficking. *Blood.* 2016;127(11):1459-67.
50. Szklarczyk D, Morris JH, Cook H, Kuhn M, Wyder S, Simonovic M, et al. The STRING database in 2017: quality-controlled protein-protein association networks, made broadly accessible. *Nucleic Acids Res.* 2017;45(D1):D362-D8.
51. Zeiler M, Moser M, and Mann M. Copy number analysis of the murine platelet proteome spanning the complete abundance range. *Mol Cell Proteom.* 2014;13(12):3435-45.

FIGURE LEGENDS

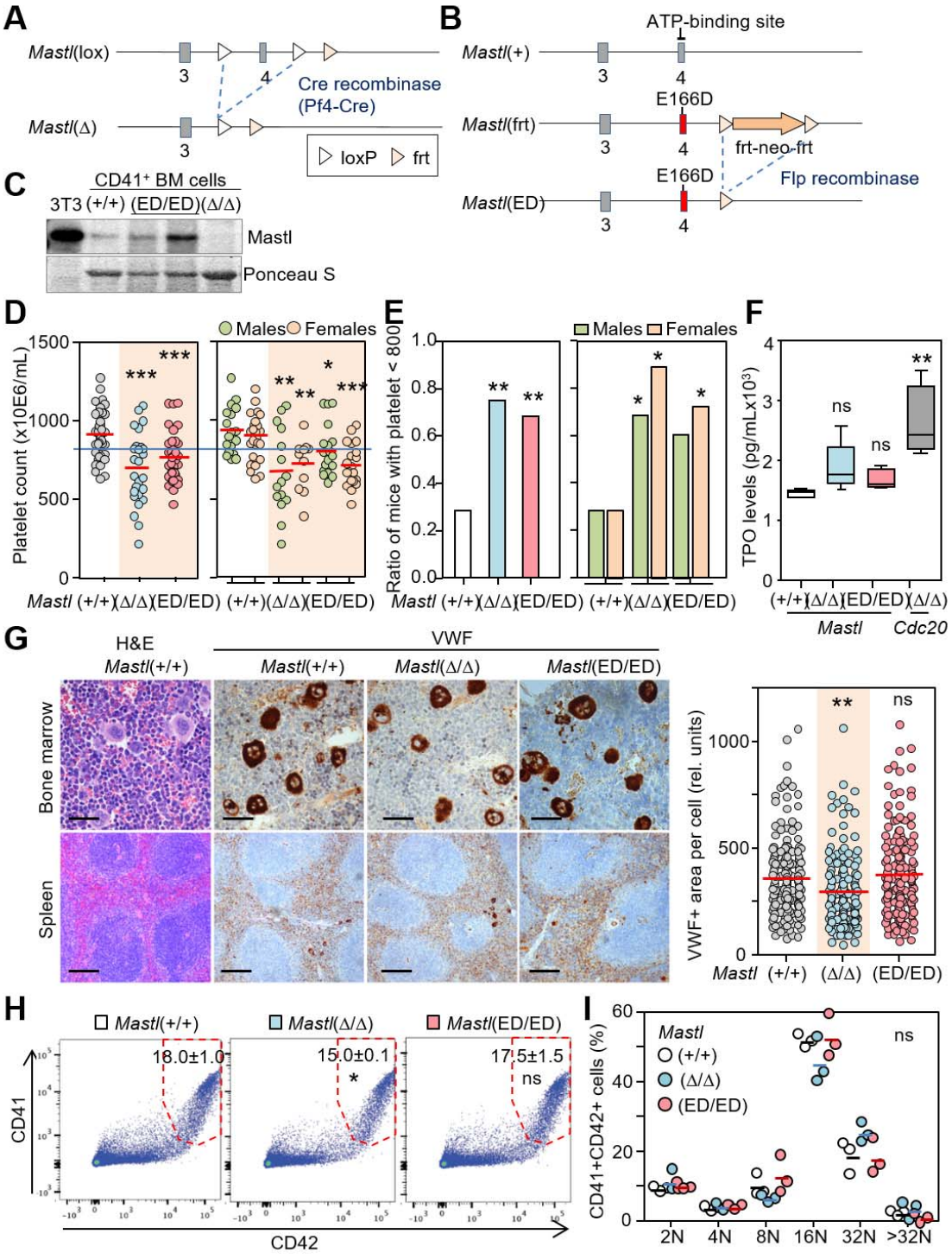

Figure 1. Mild thrombocytopenia in *Mastl*(Δ/Δ) and *Mastl*(ED/ED) mice. **A,** Representation of the *Mastl*(lox) and *Mastl*(Δ) alleles used in this work. A Pf4-Cre

transgene was used to generate megakaryocyte-specific *Mastl*-null mice. **B,** Generation of the *Mastl*(E166D) [*Mastl*(ED) for brief] allele. The frt-neo_resistance-frt cassette was removed after crossing with Flp-expressing mice. White or orange triangles represent lox or frt sequences, respectively. **C,** Expression of Mastl in bone marrow CD41+ cells from mice with the indicated *Mastl* genotypes. Lysates from NIH3T3 cells were used as a control. Representative image from two independent experiments. **D,** Platelet levels in 12-week old males (blue) or females (pink) with the indicated genotypes. The blue line indicates a concentration of $800x10^6$ platelets/ml as a reference. **E,** The percentage of mice with less than $800x10^6$ platelets/ml is shown (using mice from panel D). Males and females are represented in separated columns (right panel). **F,** Levels of thrombopoietin (TPO) in peripheral blood in the indicated mice. Cdc20-deficient mice, which display severe thrombocytopenia (33), are used as a control ($n \geq 4$ mice per genotype). **G,** Representative micrographs of bone marrow from mice with the indicated genotypes. H&E, hematoxylin and eosin; VWF, von Villebrand Factor. Images represent more than 3 mice per genotype analyzed. Scale bars, 50 μm. The quantification of the VWF signal in more than 100 megakaryocytes per genotype is indicated in the right panel. Bars indicate mean. **H,** Quantification of CD41 and CD42-positive cells in bone-marrow cells from mice with the indicated genotypes. **I,** Quantification of the ploidy in CD41+, CD42+ double positive cells from bone marrow cells of the indicated genotypes. No significant differences are found between the different genotypes (N=3 per genotype; bars indicate mean). In panels D-I, *, $P<0.05$; **, $P<0.01$; ***, $P<0.001$; ns, not significant (Student's t-test with Welch's correction in panels D,F,G and I).

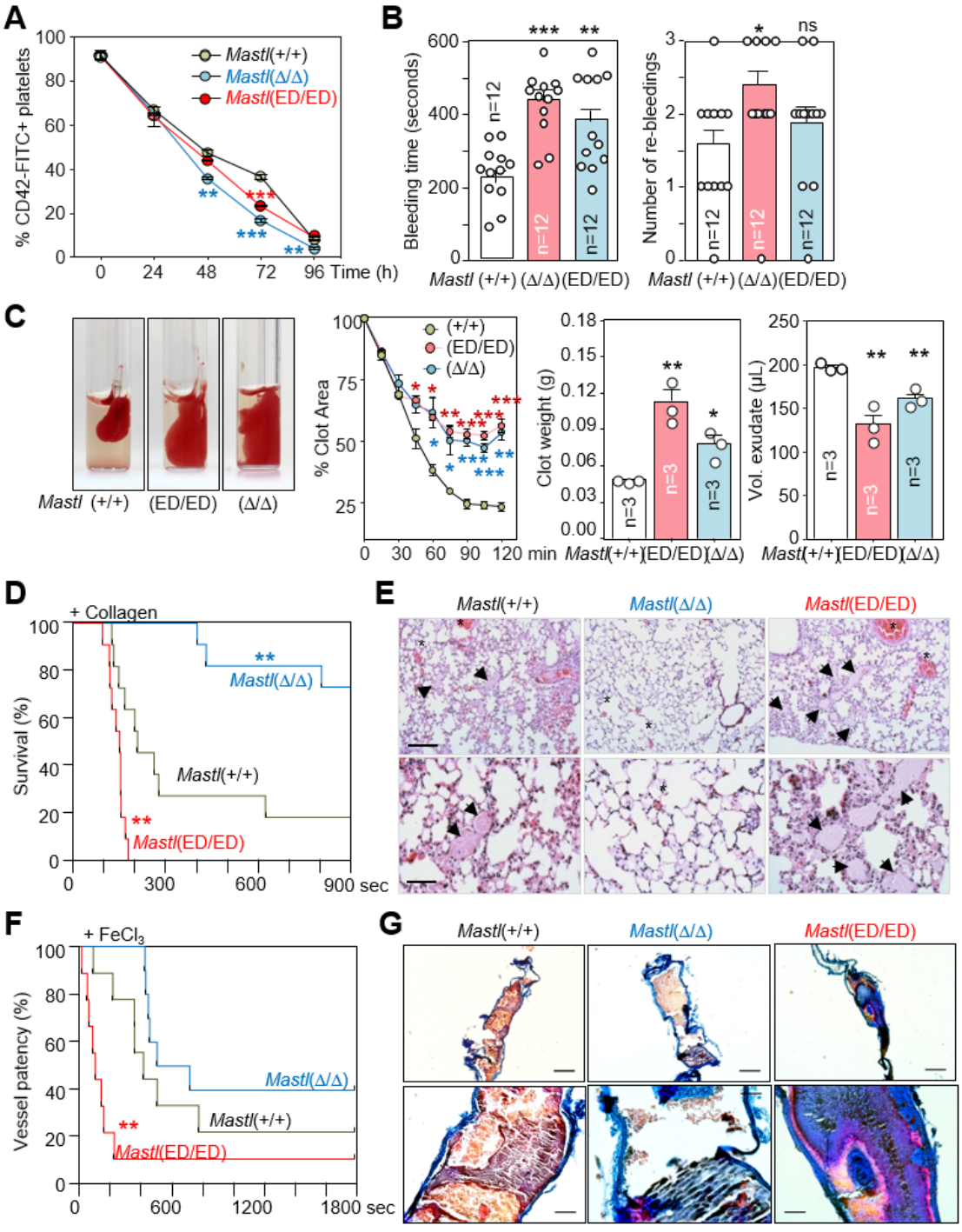

Figure 2. Altered platelet function in Mastl-mutant mice. **A,** Platelets were labeled with DyeLight488-labelled anti-CD42c (GPIbβ) antibody, then monitored for percentage of DyeLight488^{+} versus total CD41^{+} platelets, stained with an APC-labelled anti-CD41 antibody. N=3 mice per genotype. **B,** Bleeding time (left) and number of re-bleedings

(right) in mice (N=12 per genotype) with the indicated genotypes. **C,** Clot retraction in the indicated genotypes. Representative images from 3 different mice per genotype are shown on the left. The plot represents the percentage of the area of the clot versus time 0. The histograms on the right show clot weight and volume exudate (mean ± SEM) after 120 min. In panels **A**-**C**, *, $P<0.05$; **, $P<0.01$; ***, $P<0.001$; Student's t-test. **D,** Survival of control and mutant mice after induction of pulmonary embolism using collagen. N=12 mice per genotype. **, $P<0.01$; Log-rank test with Bonferroni correction. **E,** Micrographs showing thrombi (arrows) and non-coagulated blood (asterisks). Images are representative from 3 mice analyzed. Scale bars, 100 μm. **F,** Ferric chloride ($FeCl_3$)-induced carotid artery injury model. N=9 mice per genotype. **, $P<0.01$; Log-rank test with Bonferroni correction**. G,** Representative Carstairs' staining images of thrombi formed in the carotid artery after injury with 5% of $FeCl_3$ from 3 mice analyzed. Scale bars, 50 μm (above) and 10 μm (below).

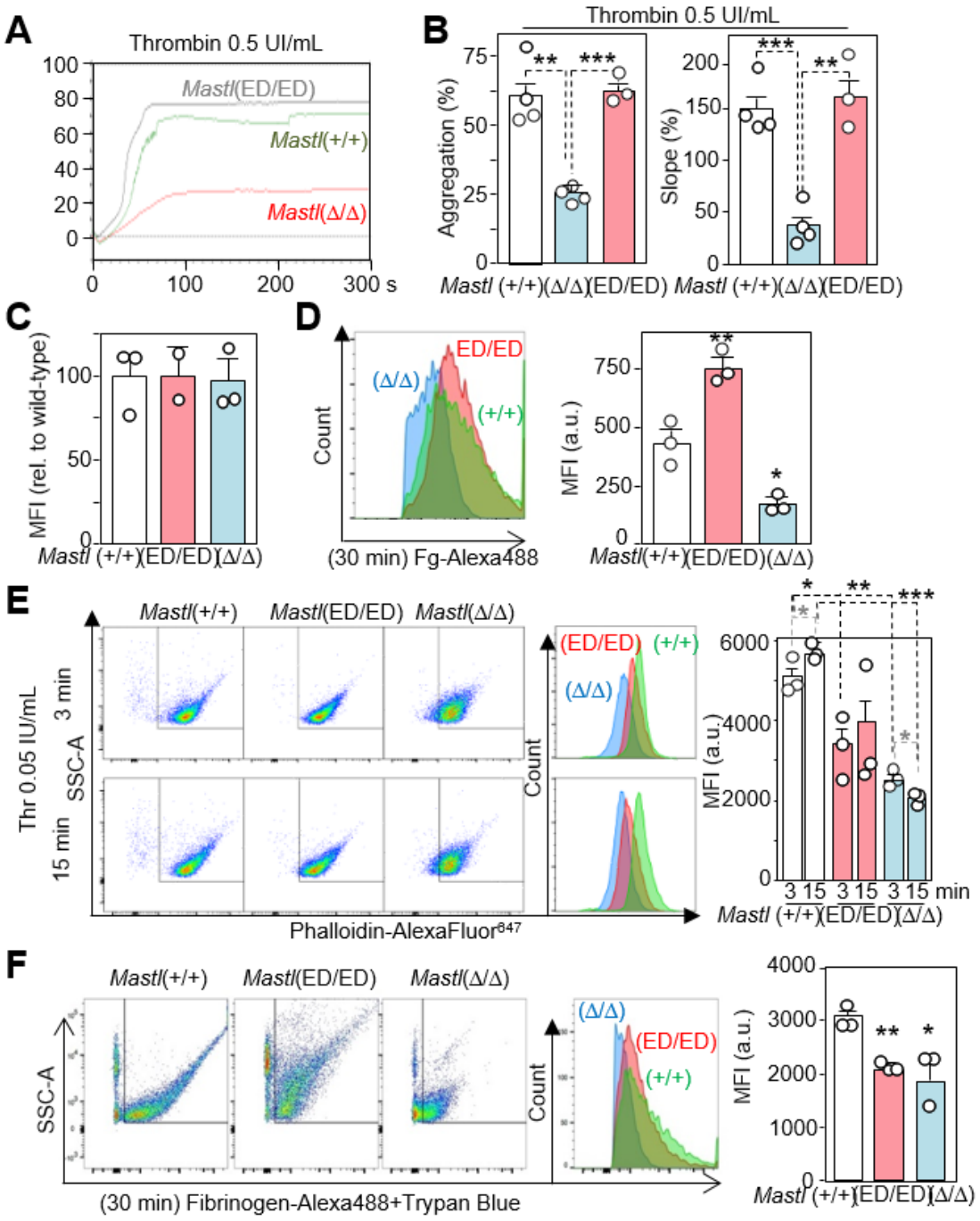

Figure 3. Platelet activation in *Mastl*(Δ/Δ) and *Mastl*(ED/ED) mutant mice. **A,** Representative light transmission aggregometry (LTA) curves of platelets with the indicated genotypes in the presence of 0.5 IU/mL of thrombin. **B,** Percentage of aggregation and slope of the aggregation curves from LTA assays. In A,B, N=4 mice per

genotype. **C,** Flow cytometry detection of activated mouse integrin αIIbβ3 (CD41a) using the specific conformational antibody JON/A (N=3 mice per genotype). **D,** Soluble fibrinogen binding quantification by flow cytometry in washed platelets activated with 0.05 IU/mL of thrombin for 30 minutes (N=3 mice per genotype). **E,** Quantification of F-Actin content by flow cytometry in activated platelets with thrombin for 3 and 15 minutes, as indicated (N=3 mice per genotype). **F,** Quantification of platelet Fibrinogen-Uptake by flow cytometry of thrombin activated platelets in presence of AlexaFluor488-labelled fibrinogen (N=4 mice per genotype). In panels **B-F**, bars represent mean ± SEM; *, $P<0.05$; **, $P<0.01$; ***, $P<0.001$ (Student's t-test).

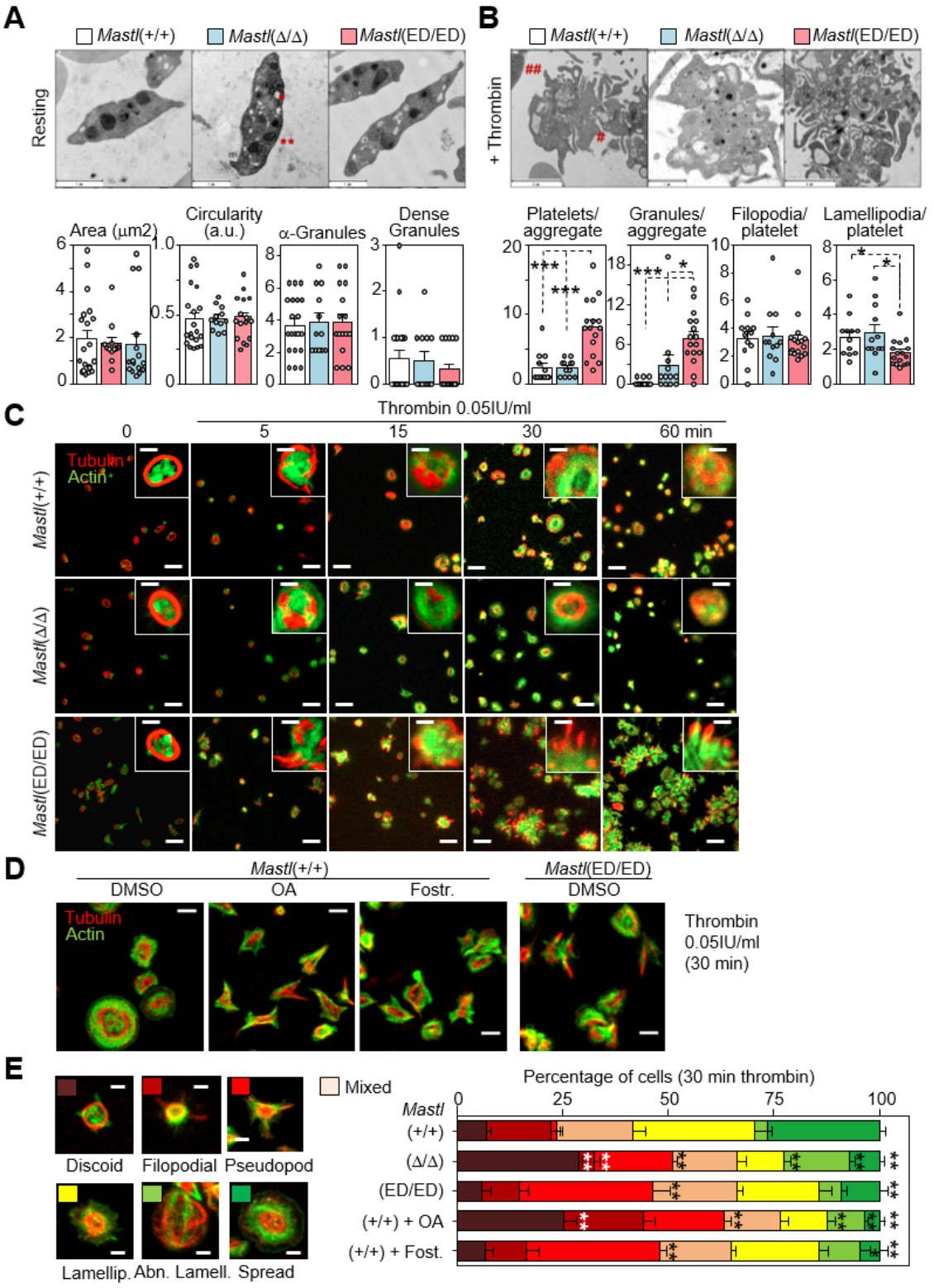

Figure 4. Platelet morphology and spreading properties in Mastl mutant mice. **A,B,** Representative electron microscopy images of resting (**A**) or activated (**B**; 0.05 IU/mL thrombin for 15 min) platelets from 3 mice with the indicated genotypes. Scale bars, 1

μm. Plots represent mean ± SEM of the quantification of the area, circularity (0-1, being 1 a perfect circle) and number of α and δ-granules per platelet (N=3 mice per genotype; Student's t-test with Welch's correction). **C,** Spreading of platelets on fibrinogen. Platelets were stained with α-tubulin (red) and Phalloidin (green). Scale bars, 10 μm. (insets: 2 μm). Images are representative of 6 independent experiments. **D,** Representative images of activated thrombin platelets spread on fibrinogen for 30 min, in presence of vehicle (DMSO 0.01%) or the phosphatase inhibitors Okadaic acid (OA, 250nM) or Fostriecin (Fos, 5μM). Platelets were stained as in C). Scale bars, 5 μm. **E,** Quantification of platelet morphology after thrombin activation on fibrinogen for 30 min. Representative images of discoid, filopodial, pseudopod, llamellipodia, abnormal llamellipodia and spread platelets are shown on the left. Scale bars, 5 μm. The plot represents the percentage (mean ± SEM; Mann-Whitney test) of cells in each category (>150 cells per experiment from 3 independent experiments). In panels A,B,E *, $P<0.05$; **, $P<0.01$; ***, $P<0.001$.

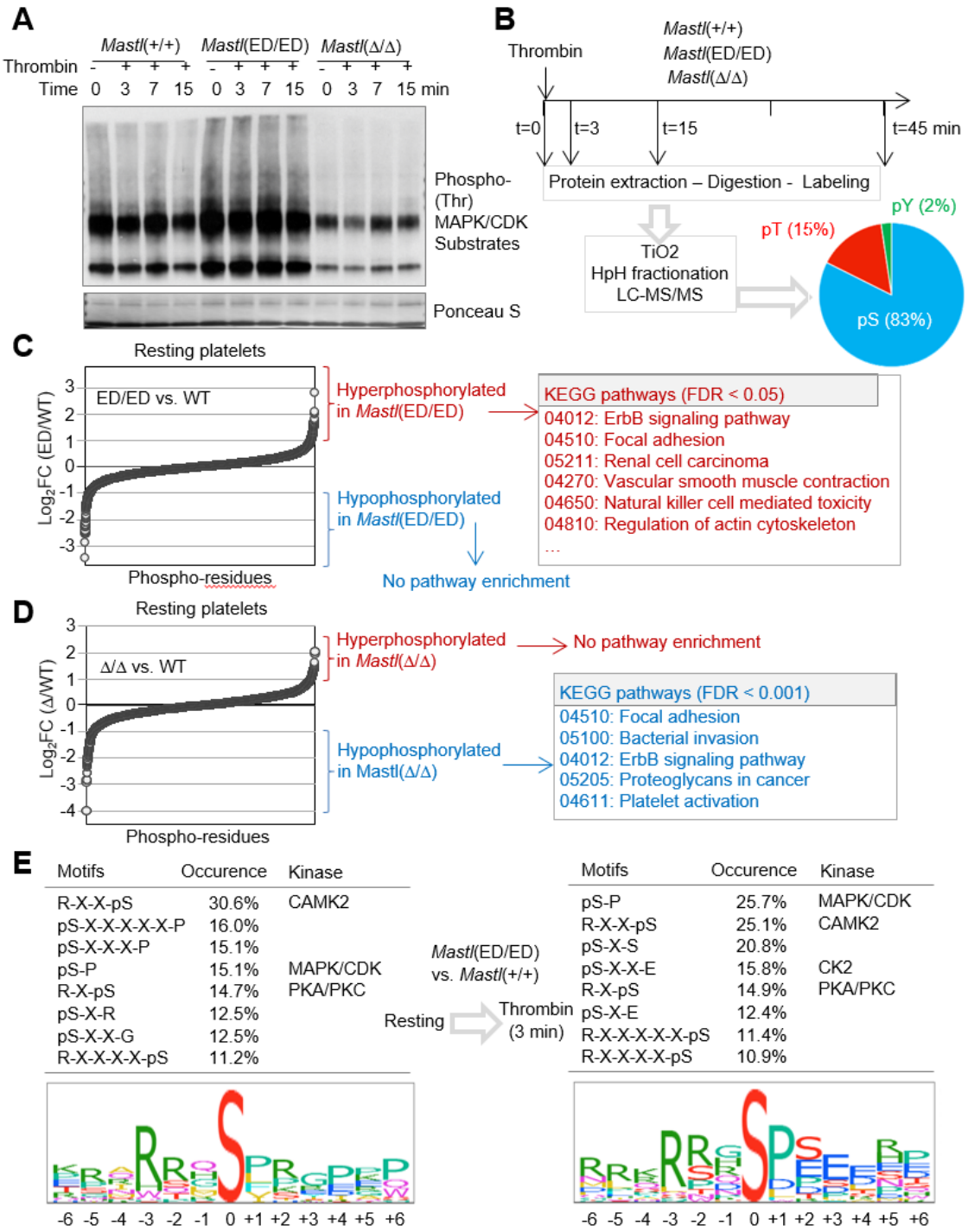

Figure 5. Phospho-proteomic analysis in Mastl-mutant platelets. **A,** Levels of phospho-MAPK/CDK substrates (proline-directed phosphosites) in resting platelets (0 min) or platelets activated with 0.05 IU/mL of thrombin for 3, 7 and 15 min from the indicated genotypes. The image represents two separate experiments. **B,** Schematic representation

of the protocol used in phophoproteomics experiments. The plot represents the percentage of peptides phosphorylated in serine (pS), threonine (pT) or tyrosine (pY) over the total of phosphopeptides detected. A pool of platelets from three mice per genotype were used in each time point. **C,D,** Fold change (log_2) of all identified phosphosites in *Mastl*(ED/ED) (**C**) or *Mastl*(Δ/Δ) (**D**) versus *Mastl*(+/+) platelets in resting conditions. The enrichment of specific KEGG pathways in hyperphosphorylated ($log_2FC \geq 0.75$) or hypophosphorylated ($log_2FC \leq -0.75$) sites was calculated using the mouse platelet proteome as background. See Supplementary Tables 2-3 for a complete list of enriched pathways. FDR=False discovery rate. **E,** Analysis of hyperphosphorylated motifs in *Mastl*(ED/ED) vs. *Mastl*(+/+) resting platelets (left) or 3 min after activation with thrombin (right) using the *de novo* motif finder tool from the Posttraslational Modification Database (PHOSIDA).

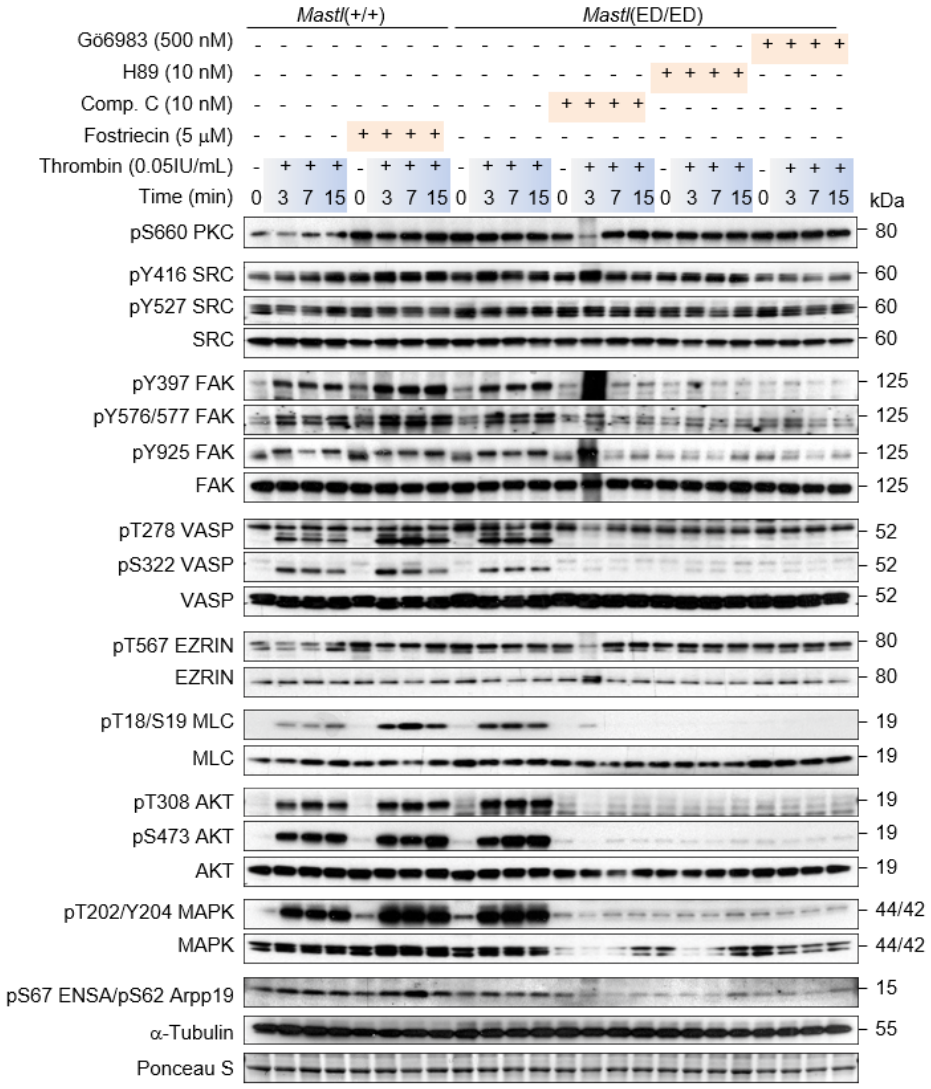

Figure 6. Activation of focal adhesion and actin dynamics pathways in Mastl-mutant platelets. Immunoblot analysis of total protein extracts from platelets in resting (0 min) or thrombin-activated conditions (3, 7 and 15 min). When indicated, platelets were pre-treated with phosphatase (Fostriecin) and kinase (Compound C, H89, Gö6983 which inhibit Ampk, Pka and Pkc, respectively) inhibitors for 15 min at 37ºC before activation. Pools of platelets from 3 mice per genotype were used in each condition. The image represents 3 separate experiments. Antibodies are referred to by their commercial name and the phosphoresidues indicated correspond to the human nomenclature.

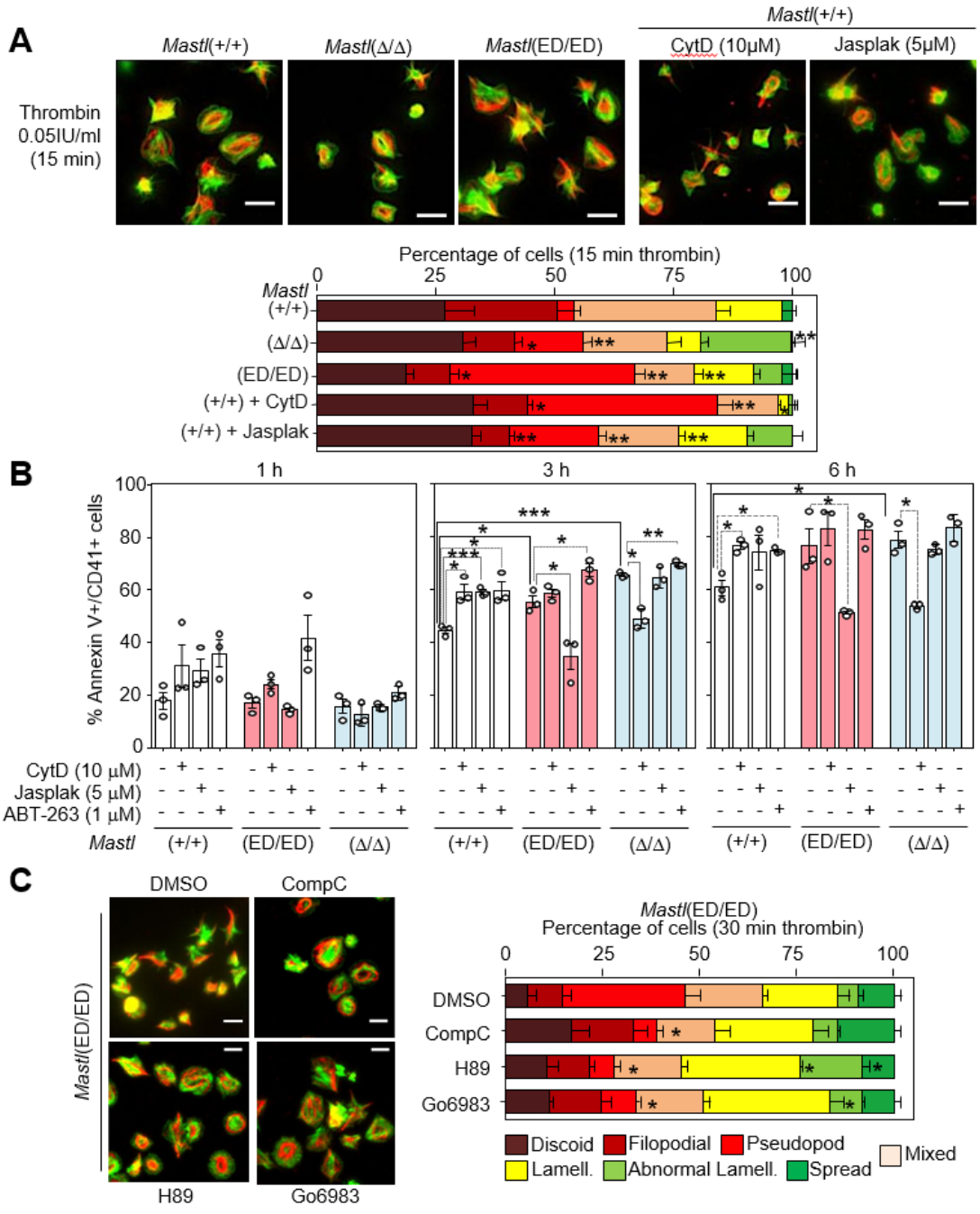

Figure 7. Platelet defects in *Mastl*(ED/ED) mutant mice are mimicked with actin polymerization inhibitors and rescued by inhibiting inside-out kinases. **A**, Representative images of wild-type platelets treated with cytochalasin D (CytD) or jasplakinolide (Jasplak) 15 min after activation with thrombin. Untreated wild-type or mutant platelets are shown as a control. **B**, Percentage of Annexin V-positive cells, as quantified by flow cytometry with specific antibodies, in platelets (as labelled with CD41-specific

antibodies) with the indicated genotypes in the absence or presence of cytochalasin D (CytD), jasplakinolide (Jasplak) or the Bcl2-family inhibitor ABT-263 (used as a control for the induction of cell death), one, three or six h after activation with thrombin. Bars represent mean ± SEM (Student's t-test with Welch's correction). **C,** Representative images of *Mastl*(ED/ED) platelets activated with 0.05 IU/mL of thrombin and spread on fibrinogen for 30 min, in presence of vehicle (DMSO 0.01%) or the kinase inhibitors Compound C (CompC 10 nM), H89 (10 nM) or Gö6983 (500 nM). In **A** and **C**, platelets were stained with α-tubulin (red) and Phalloidin (green), and plots show the percentage (mean ± SEM) of cells in the categories described in Figure 4E (n>150 cells per experiment from 3 independent experiments). Scale bars, 5 μm. In **A-C**, *, $P<0.05$; **, $P<0.01$; ***, $P<0.001$ (Mann-Whitney test).

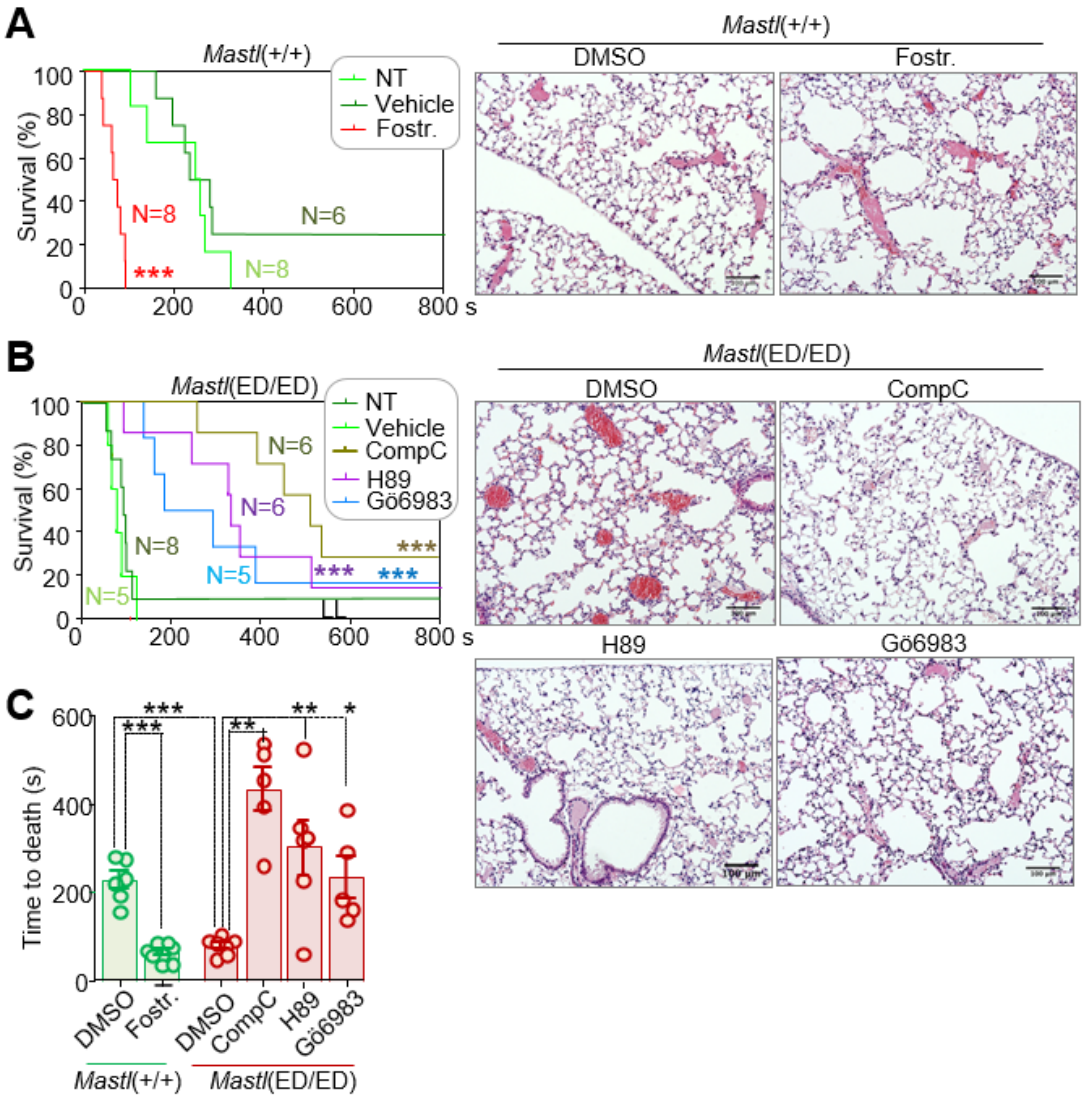

Figure 8. Functional defects in *Mastl*(ED/ED) mutant platelets are mimicked with phosphatase inhibitors and rescued by inhibiting inside-out kinases in vivo. **A,B,** Survival curves after pulmonary embolism in *Mastl*(+/+) mice treated with the phosphatase inhibitor Fostriecin (**A**), or *Mastl*(ED/ED) mice treated with kinase inhibitors (**B**) for 1 h before of the induction of pulmonary embolism. The number of mice per group is indicated in the plot. NT=non treated. ***, $P<0.001$ (Log-rank test with Bonferroni correction). Representative images of hematoxylin and eosin stained lungs are shown on the right (N=3 mice per genotype). **C,** Time to death of the experimental groups in panels

A and B. Bars represent mean ± SEM. *, $P<0.05$; **, $P<0.01$; ***, $P<0.001$ (Student's t-test with Welch's correction).